ELSEVIER

Applied Ocean Research 26 (2004) 114–136

Applied Ocean Research

www.elsevier.com/locate/apor

Statistical properties of successive wave heights and successive wave periods

Hanne T. Wist[a,*], Dag Myrhaug[a], Håvard Rue[b]

[a]Department of Marine Technology, Norwegian University of Science and Technology, N-7491 Trondheim, Norway
[b]Department of Mathematical Sciences, Norwegian University of Science and Technology, N-7491 Trondheim, Norway

Received 11 June 2004; accepted 26 January 2005
Available online 22 April 2005

Abstract

Two successive wave heights are modeled by a Gaussian copula, which is referred to as the Nataf model. Results with two initial distributions for the transformation are presented, the Næss model [Næss A. On the distribution of crest to trough wave heights. Ocean Engineering (1985);12(3):221–34] and a two-parameter Weibull distribution, where the latter is in best agreement with data. The results are compared with existing models. The Nataf model has also been used for modeling three successive wave heights.

Results show that the Nataf transformation of three successive wave heights can be approximated by a first order autoregressive model. This means that the distribution of the wave height given the previous wave height is independent of the wave heights prior to the previous wave height. Thus, the joint distribution of three successive wave heights can be obtained by combining conditional bivariate distributions. The simulation of successive wave heights can be done directly without simulating the time series of the complete surface elevation.

Successive wave periods with corresponding wave heights exceeding a certain threshold have also been studied. Results show that the distribution for successive wave periods when the corresponding wave heights exceed the root-mean-square value of the wave heights, can be approximated by a multivariate Gaussian distribution.

The theoretical distributions are compared with observed wave data obtained from field measurements in the central North Sea and in the Japan Sea, with laboratory data and numerical simulations.

Keywords: Successive wave heights; Successive wave periods; Nataf transformation; Copulas; First order autoregressive model; Field data; Laboratory data; Simulations

1. Introduction

In design and analysis of ships and offshore structures, a good description of the surface elevation is important. The surface elevation can be described by a number of parameters for individual waves, e.g. the wave height, the wave period, the wave-length and the wave steepness. It is important to find good statistical models that give accurate parameter predictions and corresponding uncertainty estimates, and, it is therefore, of interest to find both marginal probability distributions as well as joint probability distributions for combined parameters or a single parameter in successive waves.

Estimation of the probability of a wave height exceeding a critical level has long been recognized as important statistics in design and safety evaluation of coastal and offshore structures and vessels. However, when, e.g. calculating wet-deck slamming and green water loads, or when selecting the deck elevation of a fixed offshore platform, it is the wave crest height rather than the total wave height that is of interest. A number of marginal distributions for the wave crest height are available, both theoretical models and empirical models. Longuet-Higgins [1] first introduced the Rayleigh distribution for prediction of the wave amplitude in a narrow-banded random sea. Cartwright and Longuet-Higgins [2] modified the Rayleigh distribution to account for a more broad-banded random sea by including the spectral bandwidth parameter. In severe sea states, nonlinear effects must be taken into account.

* Corresponding author. Present address: Department of Mathematical Sciences, Norwegian University of Science and Technology, N-7491 Trondheim, Norway.
E-mail address: hanne.wist@math.ntnu.no (H.T. Wist).

0141-1187/$ - see front matter © 2005 Elsevier Ltd. All rights reserved.
doi:10.1016/j.apor.2005.01.002

A summary of some of the wave crest models can be found in [3]. Joint distributions of successive wave crest heights will not be discussed further in this paper, but this is thoroughly described in [4,5].

In addition to the distributions for the wave crest heights, several distributions have been proposed for the total wave height in order to improve the model of [1]. Longuet-Higgins and Næss [6,7], among others, have modified the model to give a better fit to measured wave data. A summary of some of the wave height models can be found in [8]. Several two-dimensional distributions exist for modeling two successive wave heights. These are based on transformations of well known joint distributions, e.g. the two-dimensional Rayleigh distribution [9], or the two-dimensional Weibull distribution (see, e.g. [10]). It is also of interest to consider a joint distribution for more than two successive wave heights. Extending the existing two-dimensional distributions to three-dimensional distributions or higher, is not possible, since a three-dimensional Weibull distribution is not known. Another approach must therefore be used, e.g. by using a Nataf transformation [11] as described in this paper.

Closely related to the joint distributions is the conditional distribution, e.g. to know the probability of a wave height exceeding a specified value given that the previous wave height exceeded the same value. By approximating the process of successive wave heights by a first order autoregressive (AR(1)) model, the distribution of the wave height, given the previous wave height is independent of the wave heights prior to the previous wave height. Thus, only two-dimensional distributions are required to investigate the conditional statistical properties.

The study of wave periods is relevant in analysis of ships and structures that can be excited to move near resonance. For critical wave periods, it is also of interest to know the corresponding wave height. Closely related to this is the study of conditional distributions, e.g. to know the probability distribution of two or more successive wave periods given that the corresponding wave heights exceeded a given value. This is of interest, e.g. when studying parametric roll motion of ships. Ships in head sea can, under given conditions, experience parametric roll motion when the wave encounter period is approximately half the natural period of roll motion and the wave heights are exceeding a critical level [12].

The study of marginal probability distributions for wave periods have been addressed by Bretschneider [13]. He assumed that the wave-length was proportional to the square of the wave period, and combined this with a transformation of the Rayleigh distribution. Longuet-Higgins [14,15] presented two models for the marginal probability distributions for wave periods, where both models were obtained theoretically from the joint probability density function (pdf) of the envelope amplitude and the time derivative of the envelope phase. The Longuet-Higgins model [14] was symmetric about the mean wave period, while the Longuet-Higgins model [15] was asymmetric. Cavanié et al. [16] presented a joint pdf for wave heights and wave periods that accounted for the asymmetry in the wave periods. Tayfun [17] presented a joint distribution of wave heights and wave periods that was conditioned on the wave height being above a threshold, given by the mean wave height. The resulting distribution was Gaussian with modified mean value and standard deviation.

Most theoretical models are based on the narrow-band approximation, but Lindgren and Rychlik [18] presented a joint distribution of wave heights and wave periods that also is valid for broad-banded sea states. However, the expressions involved are not in a closed form, thus numerical integration is required. Rychlik et al. [19] also presented distributions for ocean wave parameters using a transformed Gaussian model.

The study of distributions for wave heights and wave periods in sea states with two-peaked spectra have been addressed by Rodríguez and Guedes Soares using a four-parameter wave spectrum model, which is a combination of two JONSWAP spectra [20]. A series of papers have been presented on wave heights [21], wave periods [22] and wave heights and wave periods [23,24].

Fewer models have been presented for joint distribution of two successive wave periods. Kimura [9] presented a two-dimensional Weibull distribution and compared the theoretical model with data from numerical simulations. Myrhaug and Rue [25] presented a two-dimensional distribution based on the Bretschneider model [13]. A revised model was given in [26]. Myrhaug and Slaattelid [27] presented a parametric model of the joint distribution of two successive wave periods. The model was obtained as a best fit to measured wave data from the Frigg field in the Central North Sea. The data included more than 3 million individual waves. One application of these models is the study of near-resonant rolling of ships in beam seas by Myrhaug et al. [28].

2. Joint distributions of successive wave heights

2.1. Background

The sea surface elevation is assumed to be a stationary, Gaussian, narrow-banded random process. Then, according to [1], the wave height η_h is Rayleigh distributed, i.e.

$$F_H(h) = 1 - \exp\{-h^2\}; \quad h_{\text{rms}} = \frac{\eta_h}{h_{\text{rms}}} \geq 0, \tag{1}$$

where h is the dimensionless wave height and $h_{\text{rms}} = 2(2m_0)^{1/2}$ is the root-mean-square value of the linear wave height. The nth spectral moment, m_n, is defined by

$$m_n = \int_0^\infty \omega^n S(\omega) \mathrm{d}\omega; \quad n = 0, 1, 2, \ldots, \tag{2}$$

where $S(\omega)$ is the one-sided wave spectrum and ω is the angular wave frequency. Later Goda, Haring et al. and Forristall [29–31] among others, showed by comparison with data from the Japanese coasts and the Gulf of Mexico, respectively, that this choice of normalizing factor over-predicts the wave heights. Forristall [31] analyzed 116 h of hurricane generated waves from the Gulf of Mexico, and fitted a two-parameter Weibull distribution to the data. Later, Longuet-Higgins [6] showed that the same data were well predicted by the Rayleigh distribution in Eq. (1), if the normalizing factor was selected as $\tilde{h}_{\mathrm{rms}} = 1.85(2m_0)^{1/2}$. The reduction in the rms-value was explained by the finite bandwidth in the field data, which also was discussed in general by Boccotti [32].

Næss [7] used a different approach to derive an expression for the wave height in a stationary, narrow-banded Gaussian wave train. By defining $\rho_N = R_\eta(\tau/2)/R_\eta(0)$, where $R_\eta(\tau)$ is the autocorrelation function of the Gaussian wave elevation, the distribution function of the dimensionless wave height was given by

$$F_H(h) = 1 - \exp\left\{-\frac{2h^2}{1-\rho_N}\right\}; \quad h \geq 0. \tag{3}$$

The joint density function of two successive wave heights H_1 and H_2 is given by the two-dimensional Rayleigh distribution [33]

$$f_{H_1,H_2}(h_1,h_2) = \frac{4h_1h_2}{1-\kappa_h^2}\exp\left\{-\frac{h_1^2+h_2^2}{1-\kappa_h^2}\right\}I_0\left[\frac{2\kappa_h h_1 h_2}{1-\kappa_h^2}\right];$$
$$h_1 = \frac{\eta_{h1}}{h_{\mathrm{rms}}}, \quad h_2 = \frac{\eta_{h2}}{h_{\mathrm{rms}}}, \tag{4}$$

where I_0 denotes the modified Bessel function of zeroth order given by

$$I_0(z) = \frac{1}{\pi}\int_0^\pi \mathrm{e}^{z\cos\theta}\mathrm{d}\theta. \tag{5}$$

Furthermore, the parameter κ_h is related to the correlation coefficient, ρ_h, between H_1 and H_2 by

$$\rho_h \equiv \rho_{H_1,H_2} = \frac{E(\kappa_h) - \frac{1}{2}(1-\kappa_h^2)K(\kappa_h) - \frac{\pi}{4}}{1-\frac{\pi}{4}}, \tag{6}$$

where $K(\kappa_h)$ and $E(\kappa_h)$ are complete elliptic integrals of the first and second kind, respectively. Based on Næss model [7] in Eq. (3), transformation of variables combined with Eq. (4) gives the pdf of H_1 and H_2 as

$$f_{H_1,H_2}(h_1,h_2) = \frac{16h_1h_2}{(1-\kappa_h^2)(1-\rho_N)^2}\exp\left\{\frac{-2(h_1^2+h_2^2)}{(1-\kappa_h^2)(1-\rho_N)}\right\} \times I_0\left[\frac{4\kappa_h h_1 h_2}{(1-\kappa_h^2)(1-\rho_N)}\right]. \tag{7}$$

In the following, Eq. (7) will be referred to as the two-dimensional Næss model.

2.2. Successive wave heights modeled by using copulas

If the marginal distribution functions are known, then a joint distribution function can be constructed by using copulas An introduction and overview of the subject is given in [34], and a historical development can be found in [35]. It was Sklar, who first introduced the term copula in 1959. However, earlier Fréchet [36] among others, had made important contributions to the subject.

Sklar's theorem stated that if the random variables $X_1,\ldots,X_p$ have marginal distribution functions $F_{X_1},\ldots,F_{X_p}$, respectively, and joint distribution function $F_{X_1,\ldots,X_p}$, then there exists a p-dimensional copula C such that

$$F_{X_1,\ldots,X_p}(x_1,\ldots,x_p) = C(F_{X_1}(x_1),\ldots,F_{X_p}(x_p)). \tag{8}$$

If $F_{X_1},\ldots,F_{X_p}$ are all continuous, C is unique. Conversely, if C is a p-dimensional copula and $F_{X_1},\ldots,F_{X_p}$ are distribution functions, then the function $F_{X_1,\ldots,X_p}$ defined by Eq. (8) is a p-dimensional distribution function with margins $F_{X_1},\ldots,F_{X_p}$.

The Gaussian distribution is often preferable in the multivariate case. The analytical expression for the multivariate distribution allows to calculate exact statistical quantities of interest. The use of standard Gaussian distributions for the marginal distributions is often referred to as the Nataf model (see, e.g. [37]), although, Nataf [11] only described the general use of copulas.

The Nataf transformation has been used for modelling other sea state parameters that are not discussed in this paper, like the significant wave height and the peak period, see, e.g. [38,39].

The method of constructing a joint distribution function for successive wave heights will be shown in the bivariate case, and the extension to the multivariate case is trivial. A two-dimensional Gaussian copula is given by

$$C(u_1,u_2) = \Phi(\Phi^{-1}(u_1),\Phi^{-1}(u_2)), \tag{9}$$

where the standard Gaussian distribution is given by

$$\Phi(z) = \frac{1}{\sqrt{2\pi}}\int_{-\infty}^{z}\mathrm{e}^{-(1/2)t^2}\mathrm{d}t = \frac{1}{2}\left[1+\mathrm{erf}\left(\frac{z}{\sqrt{2}}\right)\right], \tag{10}$$

and erf[ ] is the error function defined by

$$y = \mathrm{erf}(x) = \frac{2}{\sqrt{\pi}}\int_0^x \mathrm{e}^{-t^2}\,\mathrm{d}t. \tag{11}$$

The inverse of $\Phi(z)$ is given by

$$\Phi^{-1}(u_Z) = \sqrt{2}\mathrm{erf}^{-1}[2u_Z - 1], \tag{12}$$

where the random variable $U_Z = \Phi(Z)$ is uniformly distributed on [0,1].

The two-dimensional distribution function of two successive wave heights H_1 and H_2 is given from Eqs. (8)

and (9) by

$$F_{H_1,H_2}(h_1,h_2) = C(F_{H_1}(h_1), F_{H_2}(h_2)) = \Phi(\Phi^{-1}[F_{H_1}(h_1)], \Phi^{-1}[F_{H_2}(h_2)]), \quad (13)$$

where the initial marginal distributions F_{H_1} and F_{H_2} are optional.

The random variable $U_H = F_H(h)$ is uniformly distributed on [0,1]. By defining $\Psi_H(h) = \Phi^{-1}(u_H)$, the pdf of H_1 and H_2 is given by

$$f_{H_1,H_2}(h_1,h_2) = \frac{\Psi'_H(h_1)\Psi'_H(h_2)}{2\pi\sqrt{1-\rho_{12}^2}}\exp\left\{-\frac{1}{2(1-\rho_{12}^2)}(\Psi_H(h_1)^2 + \Psi_H(h_2)^2 - 2\rho_{12}\Psi_H(h_1)\Psi_H(h_2))\right\}, \quad (14)$$

where ρ_{12} is the correlation coefficient between $\Psi_H(h_1)$ and $\Psi_H(h_2)$, and $'$ denotes the derivative of Ψ_H with respect to h, which is found by using the derivative of the inverse error function given by

$$\frac{\mathrm{d}}{\mathrm{d}y}\mathrm{erf}^{-1}(y) = \frac{\sqrt{\pi}}{2}\exp\{[\mathrm{erf}^{-1}(y)]^2\}. \quad (15)$$

Two different models will be presented here as initial distributions. First, the Næss model [7] in Eq. (3) is selected. Second, to improve the transformation of the data to fit the Gaussian distribution, a two-parameter Weibull distribution of the form

$$F_H(h) = 1 - \exp\left\{-\left(\frac{h}{\alpha}\right)^{\beta}\right\}; \quad h \geq 0 \quad (16)$$

will be used. One should note that the Weibull distribution is more flexible to fit the data than the Næss model [7] with only one parameter. The Weibull parameters α and β are found from maximum likelihood estimation.

By using the Næss model [7] as the initial distribution and defining $\Psi_H^N(h) = \Psi^{-1}(u_h)$ with $U_H = F_H(h)$ from Eq. (3), the resulting transformation is

$$\Psi_H^N(h) = \sqrt{2}\mathrm{erf}^{-1}\left[2\left(1-\exp\left\{-\frac{2h^2}{1-\rho_N}\right\}\right)-1\right], \quad (17)$$

with derivative

$$\Psi_H^{N'}(h) = \frac{4\sqrt{2\pi}h}{1-\rho_N}\exp\left\{\left(\mathrm{erf}^{-1}\left[1-2\exp\left\{-\frac{2h^2}{1-\rho_N}\right\}\right]\right)^2 - \frac{2h^2}{1-\rho_N}\right\}. \quad (18)$$

By using the Weibull distribution as the initial distribution and defining $\Psi_H^W(h) = \Psi^{-1}(u_H)$ with $U_H = F_H(h)$ from Eq. (16), the resulting transformation is

$$\Psi_H^W(h) = \sqrt{2}\mathrm{erf}^{-1}\left[2\left(1-\exp\left\{-\left(\frac{h}{\alpha}\right)^{\beta}\right\}\right)-1\right], \quad (19)$$

with derivative

$$\Psi_H^{W'}(h) = \sqrt{2\pi}\frac{\beta h^{\beta-1}}{\alpha^{\beta}}\exp\left\{\left(\mathrm{erf}^{-1}\left[1-2\exp\left\{-\left(\frac{h}{\alpha}\right)^{\beta}\right\}\right]\right)^2 - \left(\frac{h}{\alpha}\right)^{\beta}\right\}. \quad (20)$$

When using copulas, the resulting joint distribution function always has correct marginals. However, the dependency structure should be examined by, e.g. a paired plot.

The extension to the multivariate case is trivial, and the pdf of $\mathbf{H} = [H_1, \ldots, H_p]^{\mathrm{T}}$ is given by

$$f_{\mathbf{H}}(\mathbf{h}) = \frac{\prod_{i=1}^{p}\Psi'_H(h_i)}{(2\pi)^{p/2}|\Sigma|^{1/2}}\exp\left\{-\frac{1}{2}\Psi_H(\mathbf{h})^{\mathrm{T}}\Sigma^{-1}\Psi_H(\mathbf{h})\right\}, \quad (21)$$

where the covariance matrix, Σ, is given by

$$\Sigma = \begin{bmatrix} 1 & \rho_{12} & \cdots & \rho_{1p} \\ \rho_{12} & 1 & \cdots & \rho_{2p} \\ \vdots & & \ddots & \vdots \\ \rho_{1p} & & \cdots & 1 \end{bmatrix}. \quad (22)$$

2.3. Successive wave heights modeled by a first order autoregressive (AR(1)) model

There are two useful representations of a time series $X(t)$. One is to use an autoregressive (AR) representation. The other is a moving average (MA) representation, which will not be discussed further here. It is also possible to have a combination of the two representations. The analysis of AR and MA processes are thoroughly described in [40].

In an AR representation, the value of X at time t is dependent on the values of its own past, plus a random variable. An AR process of order r (AR(r)) of a time series with zero mean can be written as

$$X(t) = \pi_1 X(t-1) + \cdots + \pi_r X(t-r) + \epsilon(t), \quad (23)$$

where $\pi_1, \ldots, \pi_r$ are weights, and $\epsilon(t)$ is a zero mean Gaussian white noise process. If a process with mean value different from zero is desired, this can be added afterwards. The weights can be related to the autocorrelations ρ_j and partial autocorrelations ϕ_{jj}.

In addition to the mean and variance, a stationary time series is also characterized by the autocorrelation function (ACF) and the partial autocorrelation function (PACF). The ACF measures the correlation between $X(t)$ and $X(t+j)$ and can be estimated from data by

$$\hat{\rho}_j = \frac{\sum_{i=1}^{n-j}(x_i - \bar{x})(x_{i+j} - \bar{x})}{\sum_{i=1}^{n}(x_i - \bar{x})^2}. \quad (24)$$

The PACF measures the correlation between $X(t)$ and $X(t+j)$ after their mutual linear dependency on the intervening variables $X(t+1),\ldots,X(t+j-1)$ has been removed, and is estimated by

$$\hat{\phi}_{j+1,j+1} = \frac{\hat{\rho}_{j+1} - \sum_{i=1}^{j} \hat{\phi}_{ji}\hat{\rho}_{j+1-i}}{1 - \sum_{i=1}^{j} \hat{\phi}_{ji}\hat{\rho}_i} \tag{25}$$

$$\hat{\phi}_{j+1,i} = \hat{\phi}_{ji} - \hat{\phi}_{j+1,j+1}\hat{\phi}_{j,j+1-i}, \quad i = 1,\ldots,j. \tag{26}$$

Under the hypothesis that the underlying process is a white noise series, the variance of $\hat{\phi}_{jj}$ can be approximated by

$$\mathrm{Var}[\hat{\phi}_{jj}] \approx \frac{1}{n}. \tag{27}$$

The AR(1) process has the properties

$$\rho_j = \rho_1^j, \quad j \geq 1. \tag{28}$$

$$\phi_{jj} = \begin{cases} \rho_1 = \pi_1, & j = 1, \\ 0, & j \geq 2. \end{cases} \tag{29}$$

An AR(1) process has the Markov property

$$\begin{aligned} P(X(t+1) = x_{t+1} | X(0) = x_0, \ldots, X(t) = x_t) \\ = P(X(t+1) = x_{t+1} | X(t) = x_t). \end{aligned} \tag{30}$$

Thus, the value of $X(t)$ is completely determined by the knowledge of $X(t-1)$. If the process can be written as an AR(1) process, then both simulations of the process and calculation of statistics are simplified. Sobey [41] indicated that an AR(1) process agreed with wave height data from field measurements.

Consider a stochastic process of transformed successive wave heights. If the process can be approximated by an AR(1) process, it can be written as

$$\Psi_H(t) = \rho_1 \Psi_H(t-1) + \epsilon(t); \quad t = 1, 2, \ldots, \tag{31}$$

where $\{\epsilon(t)\}$ are independent Gaussian distributed variables with zero mean and variance equal to $(1-\rho_1^2)\mathrm{Var}[\Psi_H] = 1-\rho_1^2$. The initial value can be selected as, e.g. the mean value, i.e. $\Psi_H(0) = 0$. Results presented later in this paper show that the AR(1) process is a good approximation to the process of the transformed successive wave heights. A likelihood ratio test can also be performed to test if the correlation coefficients are given by Eq. (28). See [42] for further details on likelihood ratio tests.

Simulation of the transformed successive wave heights using Eq. (31) is fast and simple. The normalized wave heights are found from the simulated process Ψ_H by inverting the transformation. This gives

$$H^N = \left(-\frac{1-\rho_N}{2} \ln\left[\frac{1}{2}\left(1 - \mathrm{erf}\left[\frac{1}{\sqrt{2}} \Psi_H^N(h) \right] \right) \right] \right)^{1/2}, \tag{32}$$

when using the transformation in Eq. (17) with the Næss model [7] as initial distribution, and

$$H^{\mathrm{W}} = \alpha \left(-\ln\left[\frac{1}{2}\left(1 - \mathrm{erf}\left[\frac{1}{\sqrt{2}} \Psi_H^{\mathrm{W}}(h) \right] \right) \right] \right)^{1/\beta}, \tag{33}$$

when using the transformation in Eq. (19) with the Weibull distribution as initial distribution.

When assuming an AR(1) model, the joint distribution of more than two successive wave heights can be obtained by combining conditional bivariate distributions, e.g. the joint pdf of three successive wave heights can be written as

$$f_{H_1,H_2,H_3}(h_1,h_2,h_3) = f_{H_3|H_2}(h_3|h_2) f_{H_2|H_1}(h_2|h_1) f_{H_1}(h_1). \tag{34}$$

The conditional density functions are given by

$$f_{H_{i+1}|H_i}(h_{i+1}|h_i) = \frac{f_{H_i,H_{i+1}}(h_i,h_{i+1})}{f_{H_i}(h_i)}; \quad i = 1, 2, \tag{35}$$

where the joint pdf is given in Eq. (14), and the marginal pdf is the Weibull pdf given by

$$f_H(h) = \frac{\beta h^{\beta-1}}{\alpha^\beta} \exp\left\{ -\left(\frac{h}{\alpha} \right)^\beta \right\}. \tag{36}$$

3. Joint distributions of successive wave periods

3.1. Background

Several distribution functions for the dimensionless wave period, $t = \tau/\bar{\tau}$, have been suggested, where the choice of normalizing factor, $\bar{\tau}$, varies. Bretschneider [13] derived a distribution for the wave period based on the distribution for the wave length. The wave-length, λ_{w}, was assumed to be Rayleigh distributed, which was supported by comparison with data. Then by assuming that the wave length was proportional by the square of the wave period, as suggested by the dispersion relationship for linear waves in deep water ($\tau^2 = (2\pi/g)\lambda_{\mathrm{w}}$, where g is the acceleration of gravity), it followed that the square of the wave period was Rayleigh distributed. The normalizing factor was given as the square-root of the rms-value of τ^2, i.e. $\bar{\tau}^2 = \zeta^2 \equiv (\tau^2)_{\mathrm{rms}}$. In terms of the non-dimensional wave period $t = \tau/T_{m01}$, where $T_{m01} = 2\pi m_0/m_1$ is the mean wave period, the pdf is given by

$$f_T(t) = 4\left(\frac{T_{m01}}{\zeta} \right)^4 t^3 \exp\left\{ -\left(\frac{T_{m01}}{\zeta} \right)^4 t^4 \right\}; \quad t \geq 0. \tag{37}$$

Other probability distributions have also been proposed by Longuet-Higgins and Cavanié et al. [14–16]. However, the shape of the wave period data is not captured by any of the models. An example of typical wave period data is shown in Fig. 1(a). More results are also given in [5]. This is data from the Draupner field, which will be presented

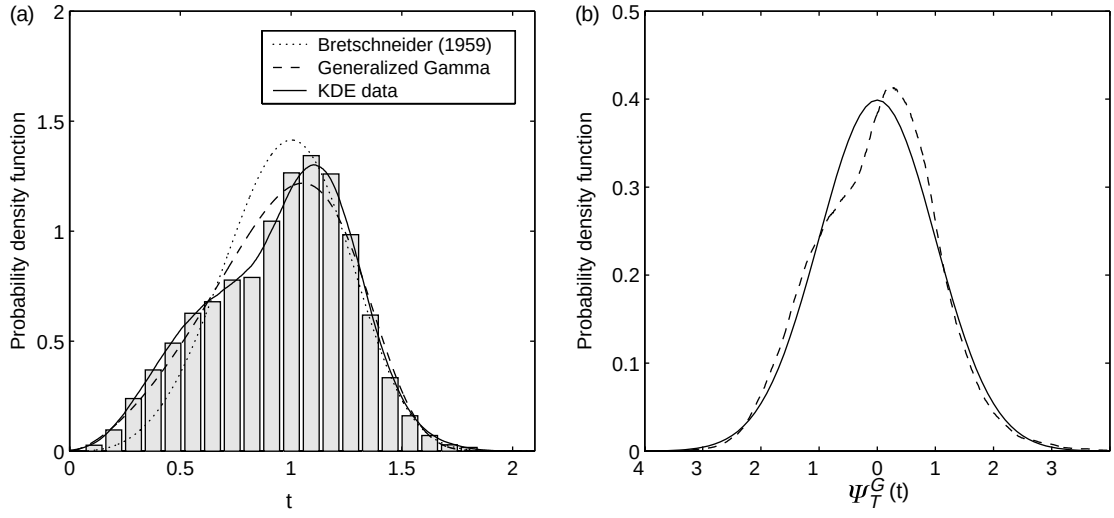

Fig. 1. (a) A histogram of the Draupner data compared with pdfs. (b) Pdf of transformed wave period data; – –, KDE of Ψ_T^G; —, standard Gaussian density function.

thoroughly later in this paper. The histogram of the data and the kernel density estimate of the data are compared with the Bretschneider model [13]. For the Draupner field data, $T_{m01} = 9.09$ s and $\zeta = 9.79$ s.

The Nataf transformation can also be applied for modeling more than two successive wave periods. A possible initial distribution is the generalized Gamma distribution. The generalized Gamma distribution was first used by Ochi [43], when modeling significant wave heights in long-term statistics. The generalized Gamma pdf is given by

$$f_T(t) = \frac{c(t-\gamma)^{c\lambda-1}}{\Gamma(\lambda)\nu^{c\lambda}} \exp\left\{-\left(\frac{t-\gamma}{\nu}\right)^c\right\}, \tag{38}$$

where λ and c are the shape coefficients, ν is the scale coefficient and γ is the location coefficient. The physical meaning of t, i.e. the wave period is always positive, implies that $\gamma = 0$. The other parameters are found from maximum likelihood estimation. For the Draupner field data, $\lambda = 0.415$, $c = 6.231$ and $\nu = 1.311$, and the resulting pdf is included in Fig. 1(a).

The generalized Gamma distribution function can be written as

$$F_T(t) = I_\Gamma\left[\lambda, \left(\frac{t}{\nu}\right)^c\right], \tag{39}$$

where I_Γ denotes the incomplete Gamma function given by

$$I_\Gamma(\lambda, u) = \frac{1}{\Gamma(\lambda)} \int_0^u \mathrm{e}^{-x} x^{\lambda-1}\, \mathrm{d}x. \tag{40}$$

Defining $\Psi_T^G(t) = \Phi^{-1}(u_T)$ with $U_T = F_T(t)$ from Eq. (39), it follows from Eq. (12) that the transformation to Gaussian density function is given by

$$\Psi_T^G(t) = \sqrt{2}\mathrm{erf}^{-1}\left\{2I_\Gamma\left[\lambda, \left(\frac{t}{\nu}\right)^c\right] - 1\right\}. \tag{41}$$

This will be denoted by the Nataf-Gamma transformation. The derivative of Ψ_T^G is given by

$$\Psi_T^{G'}(t) = \frac{\sqrt{2\pi}c}{\Gamma(\lambda)\nu}\left(\frac{t}{\nu}\right)^{c(\lambda-(1/c))} \exp\left\{\left(\mathrm{erf}^{-1}\left[2I_\Gamma\left(\lambda, \left(\frac{t}{\nu}\right)^c\right) - 1\right]\right)^2 - \left(\frac{t}{\nu}\right)^c\right\}. \tag{42}$$

Fig. 1(b) shows the kernel density estimates of the transformed wave periods compared with the standard Gaussian pdf. The figure shows that the transformation gives a poor approximation to a Gaussian distribution. The peak value is located too far to the right, and the shape of the density function does not resemble the Gaussian pdf. The difference around the peak of the density function corresponds to the shape of the marginal density function for the wave period. Unless an initial distribution that captures this feature is used, this will probably always be reflected in the transformation. Thus, both the Nataf transformation and other existing two-dimensional distributions are not able to give a good description of the data. Alternatively, one can try to fit an initial distribution that captures the behavior of the data, or one can remove the smallest values from the data set and only consider parts of the set.

Using the Nataf-Gamma transformation, the pdf for successive wave periods $\mathbf{T} = [T_1, \ldots, T_p]^{\mathrm{T}}$ is given by

$$f_{\mathbf{T}}(\mathbf{t}) = \frac{\prod_{i=1}^p \Psi_T^{G'}(t_i)}{(2\pi)^{p/2}|\Sigma|^{1/2}} \exp\left\{-\frac{1}{2}\Psi_T^G(\mathbf{t})^{\mathrm{T}} \Sigma^{-1} \Psi_T^G(\mathbf{t})\right\}, \tag{43}$$

where the covariance matrix, Σ, is given by

$$\Sigma = \begin{bmatrix} 1 & \rho_{G,12} & \cdots & \rho_{G,1p} \\ \rho_{G,12} & 1 & \cdots & \rho_{G,2p} \\ \vdots & & \ddots & \vdots \\ \rho_{G,1p} & & \cdots & 1 \end{bmatrix}, \tag{44}$$

and $\rho_{G,ij}$ is the correlation coefficient between $\Psi_T^G(t_i)$ and $\Psi_T^G(t_j)$.

Similar to the process of transformed successive wave heights, the process of transformed successive wave periods can be approximated by an AR(1) model, as described in Section 2.3. Results presented later in this paper show that the AR(1) model is a good approximation. Thus, the joint distribution of more than two successive wave periods can be obtained by combining conditional bivariate distributions, e.g. the joint pdf of three successive wave periods can be written as

$$f_{T_1,T_2,T_3}(t_1,t_2,t_3) = f_{T_3|T_2}(t_3|t_2) f_{T_2|T_1}(t_2|t_1) f_{T_1}(t_1). \tag{45}$$

The conditional density functions are given similarly as for the wave heights in Eq. (35), where the joint pdf is given in Eq. (43) with $p=2$, and the marginal pdf is given by Eq. (38).

3.2. Successive wave periods for large wave heights

Usually, the most critical situations will occur when the wave height is large. That means that it is of interest to study the probability distributions for the wave period given that the corresponding wave height exceeds a given value, e.g. h_{rms} or the significant wave height, $H_{m0}=4\sqrt{m_0}$, where the latter is of most practical interest. There exist several joint distributions of wave height and wave period.

Longuet-Higgins [14] applied a narrow-band approximation to linear theory of Gaussian noise to obtain the joint pdf of the envelope amplitude and the time derivative of the envelope phase. The joint density function of the dimensionless wave height, H, and dimensionless wave period, T, was obtained from transformation of variables. The integral of this density function is only equal to one, if negative values of the wave period is included. A new joint density function was presented by Longuet-Higgins [15], where it was taken into account that the wave period is always positive.

The conditional pdf of T given that H exceeds $\tilde{h}$ is found by integration and is given by

$$f_{T|H}(t|h>\tilde{h}) = \frac{2}{\exp(-\tilde{h}^2)\sqrt{\pi}\epsilon_2}\left[\frac{1}{2}\frac{\tilde{h}}{\tilde{t}_1\,\mathrm{e}^{\tilde{t}_1\tilde{h}^2}} + \frac{\sqrt{\pi}}{4\tilde{t}_1^{3/2}} - \frac{1}{4}\frac{\sqrt{\pi}\mathrm{erf}\left(\tilde{h}\sqrt{\tilde{t}_1}\right)}{\tilde{t}_1^{3/2}}\right], \qquad \tilde{t}_1 = 1+\left(\frac{t-1}{\epsilon_2}\right)^2, \tag{46}$$

for the Longuet-Higgins model [14] and

$$f_{T|H}(t|h>\tilde{h}) = \frac{4}{C_L\sqrt{\pi}\epsilon_2\left[1+\left(1+\epsilon_2^2\right)^{-1/2}\right]t^2} \times\left[\frac{1}{2}\frac{\tilde{h}}{\tilde{t}_2\,\mathrm{e}^{\tilde{t}_2\tilde{h}^2}} + \frac{\sqrt{\pi}}{4\tilde{t}_2^{3/2}} - \frac{1}{4}\frac{\sqrt{\pi}\mathrm{erf}\left(\tilde{h}\sqrt{\tilde{t}_2}\right)}{\tilde{t}_2^{3/2}}\right], \qquad \tilde{t}_2 = 1+\left(\frac{1-\frac{1}{t}}{\epsilon_2}\right)^2, \tag{47}$$

for the Longuet-Higgins model [15], where C_L is a normalizing constant, and ϵ_2 is the spectral bandwidth parameter given by

$$\epsilon_2 = \sqrt{\frac{m_0 m_2}{m_1^2}-1}. \tag{48}$$

Tayfun [17] presented a joint pdf of wave height and wave period that was valid for large wave heights, given by

$$f_{H,T}(h,t) = C_T h\left(1+\frac{1-\kappa_{\mathrm{a}}^2}{32\kappa_{\mathrm{a}}h^2}\right) \times\exp\left\{-\frac{1}{2}\left[\frac{4h^4}{1+\kappa_{\mathrm{a}}}+\left(\frac{t-\mu_{t|h}}{\sigma_{t|h}}\right)^2\right]\right\}, \tag{49}$$

where

$$\mu_{t|h} = 1+\epsilon_2^2(1+\epsilon_2^2)^{-3/2} \tag{50}$$

$$\sigma_{t|h} = \frac{2\epsilon_2}{\sqrt{8}h(1+\epsilon_2^2)}, \tag{51}$$

and C_T is a normalizing factor. The parameter κ_{a} is related to the correlation coefficient, ρ_{a}, between two successive linear wave amplitudes, and the relationship is equal to Eq. (6) when replacing κ_h with κ_{a} and ρ_h with ρ_{a}. The model is valid for $h>\mu_h$, the mean wave height. The conditional pdf given that $h>\tilde{h}$ must be calculated numerically.

In the Tayfun model [17], the distribution for the wave period conditioned on a given value of the wave height was approximated by a Gaussian distribution. Results presented later in this paper show that a Gaussian distribution is a good approximation also when conditioning on the wave height being larger than a given value. Thus, a transformation of the data is not necessary. The joint pdf of p successive wave periods $\boldsymbol{T}=[T_1,\ldots,T_p]^{\mathrm{T}}$, given the corresponding wave heights exceeding the level $\tilde{h}$, is then given by the multivariate Gaussian pdf

$$f_{\mathbf{T}|\mathbf{H}}(\mathbf{t}|\mathbf{h}>\tilde{h}) = \frac{1}{(2\pi)^{p/2}|\Sigma_{t|\tilde{h}}|^{1/2}}\exp\left\{-\frac{1}{2}(\mathbf{t}-\boldsymbol{\mu}_{t|\tilde{h}})^T\sum\nolimits_{t|\tilde{h}}^{-1}(\mathbf{t}-\boldsymbol{\mu}_{t|\tilde{h}})\right\}, \tag{52}$$

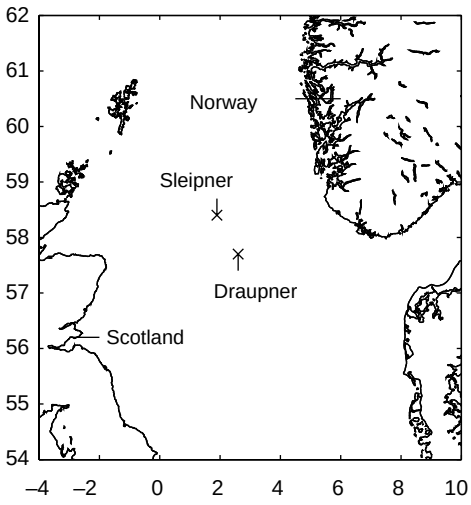

Fig. 2. Map of the Central North Sea with the Draupner platform at 57.7°N, 2.6°E, and the Sleipner platform at 58.4°N, 1.9°E.

where $\boldsymbol{\mu}_{t|\tilde{h}} = [\mu_{t|\tilde{h},1},\ldots,\mu_{t|\tilde{h},p}]^{\mathrm{T}}$ is the mean value of the wave periods given the threshold value $\tilde{h}$, and

$$\Sigma_{t|\tilde{h}} = \begin{bmatrix} \sigma^2_{t|\tilde{h},1} & \mathrm{Cov}[T_1,T_2|\tilde{h}] & \cdots & \mathrm{Cov}[T_1,T_p|\tilde{h}] \\ \vdots & & \ddots & \vdots \\ \mathrm{Cov}[T_1,T_p|\tilde{h}] & & \cdots & \sigma^2_{t|\tilde{h},p} \end{bmatrix}. \tag{53}$$

where $\mathrm{Cov}[T_i,T_j|\tilde{h}] = \rho_{ij}\sigma_{t|\tilde{h},i}\sigma_{t|\tilde{h},j}$.

The process of successive wave periods could be approximated by an AR(1) model, which has the Markov property. The Markov property will then also apply for the model of successive wave periods with corresponding large wave heights.

4. Results and discussion

4.1. Data description

Field data from the Draupner field and the Japan Sea, and laboratory data from HR Wallingford will be used for comparison with the theoretical models. Numerical simulations are also made for the different cases for comparison.

Time series were measured at the Draupner platform in the Central North Sea in the period from 31st of December 1994 to 20th of January 1995. Fig. 2 shows the location of the platform. In the same time period, wind measurements were taken at the Sleipner field, which is located approximately 70 km northwest of the Draupner platform. It is assumed that the wind conditions at the two locations are similar. The measured wind directions show that half of the data represent wind from the North, and the other half represent wind from the South. No information regarding the directional spreading of the waves is available for the data. Sunde [44] gives a description of the meteorological conditions for January 1, 1995. A discussion of the data can also be found in [4,5,45].

The data were measured by a down-looking laser sensor mounted on the Draupner jacket platform, and the waves are not expected to be seriously influenced by the structure of the platform. However, the finite water depth of 70 m does affect some waves, but overall the effect is considered to be insignificant. Thus, the data can be considered to be taken as representing deep water waves. Measurements are done during 20 min in 3-hour intervals, with a sampling frequency of 2.1333 Hz.

Analysis of the 48 individual time series show a similar statistical behavior. The values for H_{m0} vary between 6 and 8 m, the zero-upcrossing period, $T_{m02} = 2\pi\sqrt{m_0/m_2}$, varies between 7.8 and 9.1 s, and the peak frequency, ω_p, varies between 0.47 and 0.64 rad/s. Thus, the data are considered as one single time series with a total record length of 15 h and 53 min, including about 6300 individual zero-crossing waves. Fig. 3(a) shows the spectral density for this time series, where the dotted line indicates the peak frequency. The spectrum for the field data corresponds to a JONSWAP spectrum with peakedness parameter $\gamma_J \approx 1.9$, and the JONSWAP spectrum is shown in the same figure, with a broken line. The descriptive statistics of the data are given in Table 1, where T_p is the peak period.

The Japan Sea field data were obtained from measurements of the surface at the Poseidon platform, situated 3 km

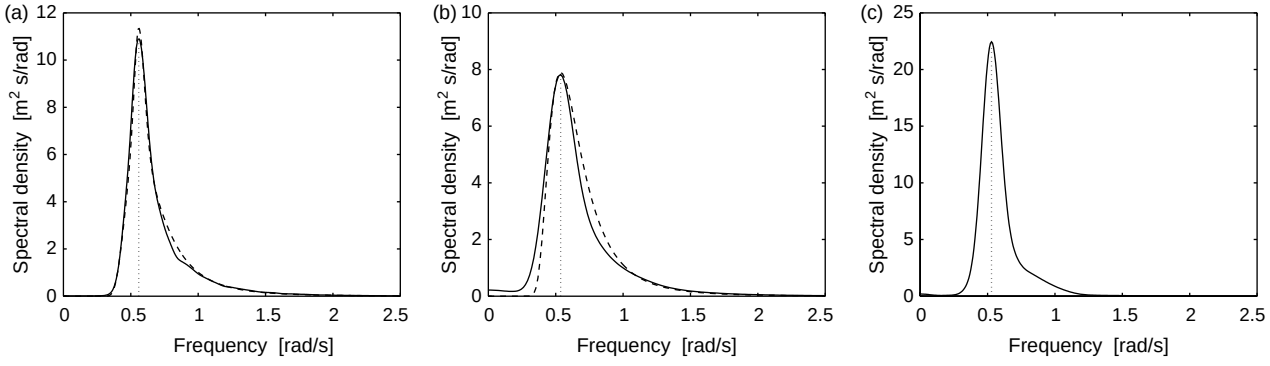

Fig. 3. The spectral density of field data (solid), peak frequency of field data (dotted). (a) Draupner data, $\omega_p = 0.56$ rad/s; JONSWAP spectrum with $\gamma_J = 1.9$ (broken). (b) Japan data, $\omega_p = 0.54$ rad/s; JONSWAP spectrum with $\gamma_J = 1$ (broken). (c) Laboratory data, $\omega_p = 0.53$ rad/s.

Table 1
Descriptive statistics of the Draupner field data, the Japan Sea field data and the laboratory data

	Draupner data	Japan data	Lab. Data
H_{m0} (m)	6.76	6.88	8.87
T_{m02} (s)	8.37	8.55	10.35
T_{m01} (s)	9.09	9.45	10.76
T_p (s)	11.23	11.70	11.87
ϵ_2 (–)	0.425	0.470	0.283

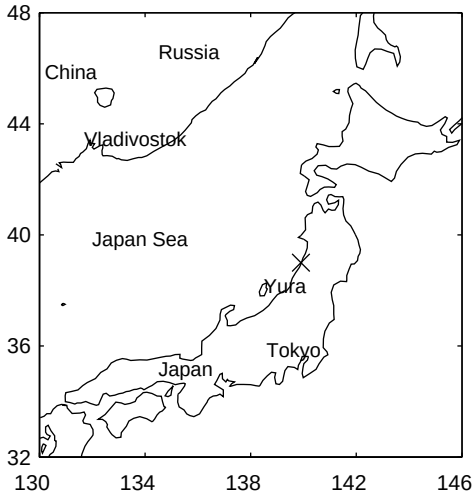

Fig. 4. Map of the Japan Sea. The Poseidon platform is situated 3 km off Yura.

off Yura. Fig. 4 is a map of the Japan Sea. In order to investigate statistical properties of a relatively heavy sea state, a 4-hour time series measured 17th of December 1987 is considered. Three intervals containing some spurious data are removed from the data set leaving a time series of 3 h and 51 min, which contains 1496 zero-upcrossing waves. The data were measured with an ultrasonic wave gauge situated at the sea floor, and the sampling frequency is 1 Hz. A cubic spline is used to interpolate the data set before further analysis. The water depth is 42 m, so a finite water depth effect is expected. Fig. 3(b) shows the spectral density for the time series. The dotted line indicates the peak frequency. A JONSWAP spectrum with peakedness parameter $\gamma_J = 1$ is shown in the same figure as the broken line. The JONSWAP spectrum tends to zero for small frequencies as opposed to the spectral density for the field data. The energy in the lowest part of the spectrum corresponds to the difference frequency effect, and this effect increases as the water depth decreases. Table 1 shows the descriptive statistics for the time series. The measured values indicate that this sea state is quite similar to the sea state for the Draupner field data. Some other aspects of the data are given in [5].

In 1997, a series of experiments in the UK Coastal Research Facility (UKCRF) at HR Wallingford were made. It should be noted that the present models cover the wave conditions at a water depth with a given constant value, and not conditions over a changing water depth. Thus, no shoaling effects are included. One should also note that the results from laboratory experiments can be influenced by effects in a closed basin, such as reflection from the edges, water flowing back from the shore or standing waves in the basin. A thorough description of the UKCRF is given in [46]. The basin is 36 m wide and has a maximum water depth of 80 cm. Long-crested (2D) as well as short-crested (3D) waves were generated according to a given peak period, a significant wave height and a wave spectrum. The water depth was constant for a length of 8.36 m after the wave generator, and then the beach rises at a slope ratio of 1:20. Seven wave probes measuring the surface elevation were located at different water depths along the tank. Fig. 5 shows the experimental setup.

In this paper, only measurements made at water depth $d = 78$ cm are analyzed. This represents relatively deep water. Similar analysis at the water depth $d = 80$ cm, and at $d = 41$ and 31 cm, representing intermediate water depths, are given in [5]. Only long-crested (2D) waves are considered. Other aspects of data collected during the same experiments are given in [47]. A time series of irregular waves was generated from a JONSWAP spectrum with spectral parameter $\gamma_J = 3$. The nominal peak period was $T_p = 1.2$ s, and the nominal significant wave height was $H_{m0} = 9$ cm. In full scale, typically 1:100, this corresponds to a sea state with $T_p = 12$ s, and $H_{m0} = 9$ m. The following results will be presented in full scale 1:100. The sampling frequency was 25 Hz with a sampling interval of 1020 s,

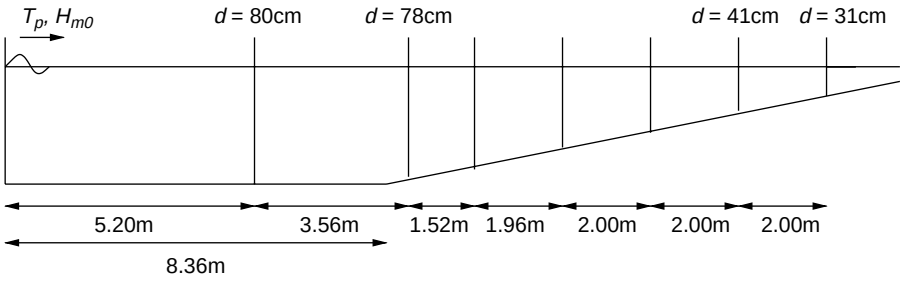

Fig. 5. Experimental setup at HR Wallingford.

Table 2
Parameters for the wave height models

	Draupner data	Japan data	Lab. data
h_{rms} (m)	4.78	4.87	6.27
ρ_N (–)	−0.689	−0.630	−0.808
κ_h^2 (–)	0.436	0.343	0.543
α (–)	0.978	0.969	0.985
β (–)	2.039	2.071	1.985

Table 3
Correlation coefficients between $\Psi_H^N(h_1)$ and $\Psi_H^N(h_i)$ and between $\Psi_H^{\mathrm{W}}(h_1)$ and $\Psi_H^{\mathrm{W}}(h_i)$, and correlation coefficients of the normalized wave heights $\rho_{h,1i}$, $i=2, 3, 4$

Draupner data	$\rho_{N,12}$	0.389	$\rho_{\mathrm{W},12}$	0.388	$\rho_{h,12}$	0.411
	$\rho_{N,13}$	0.116	$\rho_{\mathrm{W},13}$	0.116	$\rho_{h,13}$	0.126
	$\rho_{N,14}$	0.058	$\rho_{\mathrm{W},14}$	0.058	$\rho_{h,14}$	0.058
Japan data	$\rho_{N,12}$	0.294	$\rho_{\mathrm{W},12}$	0.294	$\rho_{h,12}$	0.321
	$\rho_{N,13}$	0.079	$\rho_{\mathrm{W},13}$	0.078	$\rho_{h,13}$	0.077
	$\rho_{N,14}$	0.026	$\rho_{\mathrm{W},14}$	0.026	$\rho_{h,14}$	0.022
Lab. Data	$\rho_{N,12}$	0.486	$\rho_{\mathrm{W},12}$	0.485	$\rho_{h,12}$	0.516
	$\rho_{N,13}$	0.153	$\rho_{\mathrm{W},13}$	0.153	$\rho_{h,13}$	0.170
	$\rho_{N,14}$	0.074	$\rho_{\mathrm{W},14}$	0.074	$\rho_{h,14}$	0.079

corresponding to 2 h 50 min in full scale. Table 1 shows the descriptive statistics of the full scale time series. The spectral density is shown in Fig. 3(c).

Numerical simulations using second order wave theory in [48] are made for the different cases for comparison. For each case, 10 simulations, with length equal to the length of the corresponding time series of the field data or the laboratory data, were made with identical input parameters in order to examine the variation in the results. The mean values of the simulated data are in good agreement with the corresponding values of the field data and the laboratory data. See [5] for further comparison of the wave parameters and the wave spectra between the numerical simulations and the field data and the laboratory data.

4.2. Successive wave heights

Table 2 shows the calculated parameters for the wave height models for the field data and the laboratory data. The parameter κ_h^2 is based on the values of the correlation coefficient $\rho_{h,12}$ given in Table 3.

The normalized wave height data are compared with the Rayleigh distribution in Fig. 6 in terms of the probability of exceedance. The Næss model [7] and a two-parameter Weibull distribution are also included in the figure. The figure shows that the Weibull distribution agrees best with the data in the range $h \approx 0.5$–2, where the largest concentration of data points is located. For the larger wave heights, the Næss model [7] appear to be in good agreement with the data. The simulated data agree well with the field data and the laboratory data.

Fig. 7 shows kernel density estimates of the transformed wave heights, both by using the Weibull distribution, Ψ_H^{W}, and the Næss model [7], Ψ_H^N, as initial distributions. The transformations will in the following be referred to as the Nataf-Weibull model and the Nataf–Næss model, respectively. The kernel density estimates are compared with the standard Gaussian pdf for both the field data and the laboratory data. The figures show that both transformations yield an approximate standard Gaussian distribution. The Nataf–Weibull model agrees best with the standard Gaussian distribution, while the Nataf–Næss model is slightly skewed to the left.

The correlation coefficients of the transformed wave heights are shown in Table 3. Note that the Nataf–Weibull model and the Nataf–Næss model give almost identical results. The results show that the dependency between the transformed wave heights decreases rapidly. The correlation coefficients of the normalized wave heights are also included for comparison. They are quite similar to the correlation coefficients of the transformed wave heights. Both the field data and the laboratory data show a similar behavior.

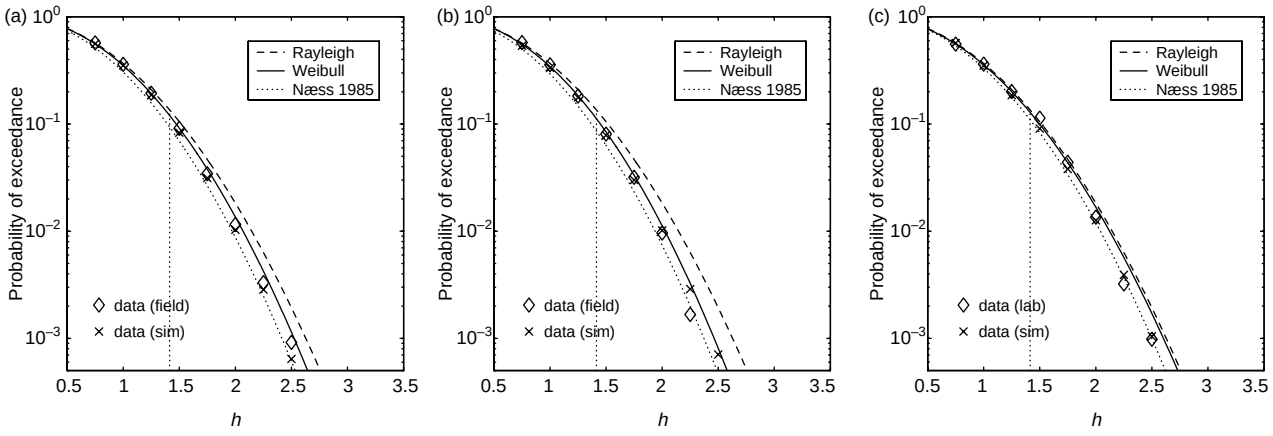

Fig. 6. Probability of exceedance for an individual wave ($P(H>h)$); (a) Draupner data; (b) Japan data; (c) Laboratory data. The normalized significant wave height equal to $\sqrt{2}$ is indicated by the vertical dotted lines.

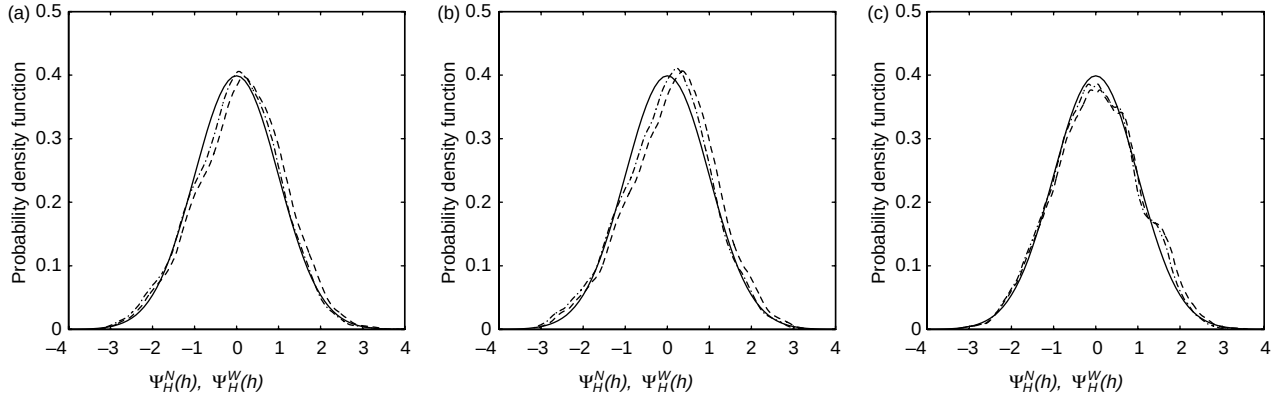

Fig. 7. Pdf of transformed wave height data; – –, kernal density estimated of Ψ_H^N; –·–, kernal density estimated of Ψ_H^W; —, standard Gaussian density function. (a) Draupner data; (b) Japan data; (c) Laboratory data.

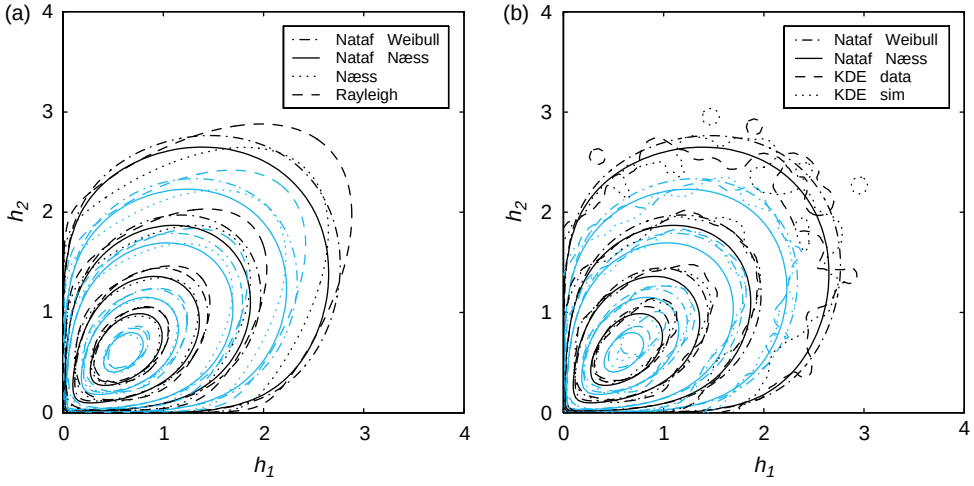

Fig. 8. Contour plot of the two-dimensional pdfs for the Draupner data. The Nataf models are compared with (a) the Rayleigh distribution and the Næss model; and (b) the kernel density estimate of the field data and one simulated time series. Percent levels of the given contour lines enclosed are 10, 30, 50, 70, 90, 95, 99 and 99.9.

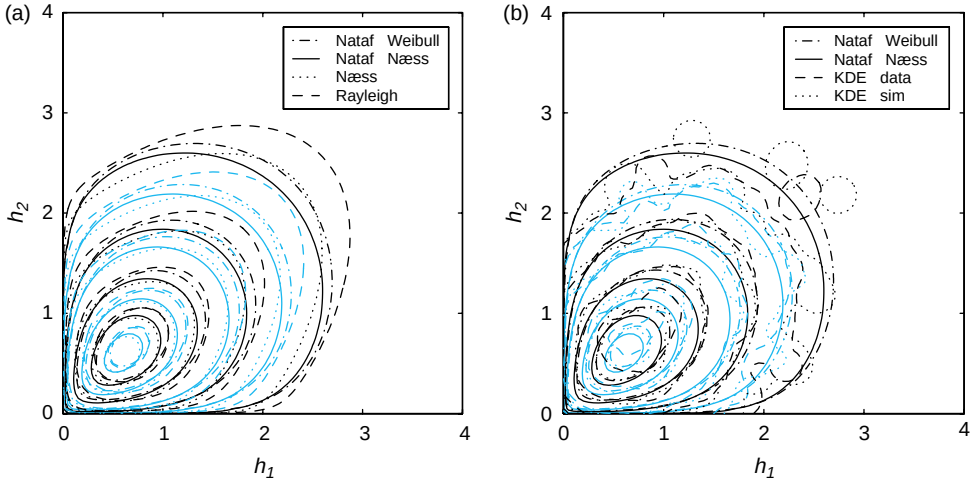

Fig. 9. Contour plot of the two-dimensional probability density functions for the Japan data. The Nataf models are compared with (a) the Rayleigh distribution and the Næss model; and (b) the kernel density estimate of the field data and one simulated time series. Percent levels of the given contour lines enclosed are 10, 30, 50, 70, 90, 95, 99 and 99.9.

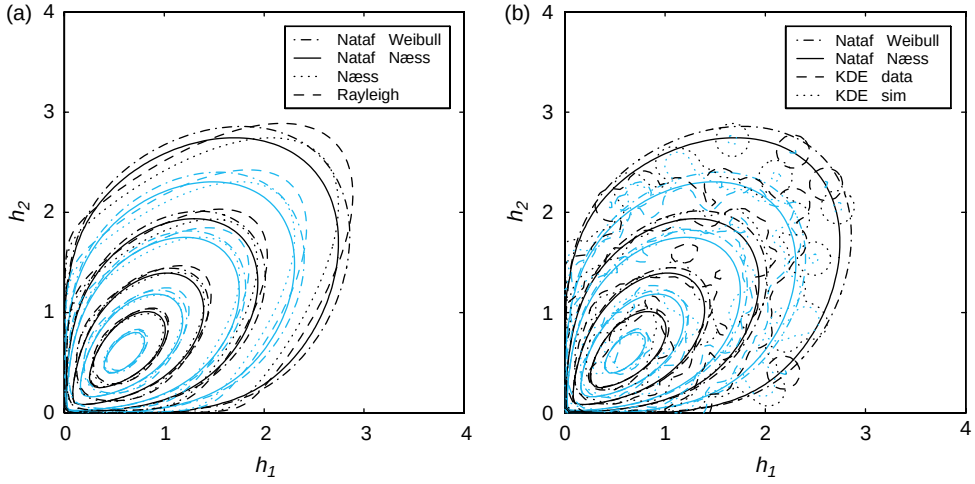

Fig. 10. Contour plot of the two-dimensional probability density functions for the laboratory data. The Nataf models are compared with (a) the Rayleigh distribution and the Næss model; and (b) the kernel density estimate of the field data and one simulated time series. Percent levels of the given contour lines enclosed are 10, 30, 50, 70, 90, 95, 99 and 99.9.

Fig. 8(a) shows a contour plot of the two-dimensional Nataf–Weibull model and Nataf–Næss model based on the parameters from the Draupner data. The distributions are compared with the two-dimensional Rayleigh distribution (Eq. (4)), and the two-dimensional Næss model (Eq. (7)). The shape of the Nataf models are somewhat different from the Rayleigh distribution and the Næss model. For larger values of h, the Nataf models have an almost circular shape, while the Næss model and the Rayleigh distribution have a more elliptic shape. Around the peaks, the distributions are quite similar. Along the diagonal ($h_1 = h_2$), the Nataf–Weibull model is close to the Rayleigh distribution for small values of h, but follows the Næss model for larger values of h. Outside the diagonal, the Nataf–Weibull model is closest to the Rayleigh distribution for all values of h. Along the diagonal, the Nataf–Næss is close to the Næss model for small values of h, but it decreases more rapidly than the other models for larger values of h. The Japan data and the laboratory data produce similar results, which are shown in Figs. 9(a) and 10(a).

The Nataf models are compared with the kernel density estimate of the Draupner data in Fig. 8(b). A kernel density estimate of one of the simulated time series is included for comparison. The models agree quite well with the field data and the simulated data. Compared with the other models in Fig. 8(a), the Nataf models with their circular shape give a better prediction of the data outside the diagonal. None of the distributions predict the peak of the data correctly, but the Nataf–Weibull model gives a slightly better prediction of the peak than the Nataf–Næss model. Overall, the Nataf–Weibull model gives the best agreement with the data. The corresponding results for the Japan data and the laboratory

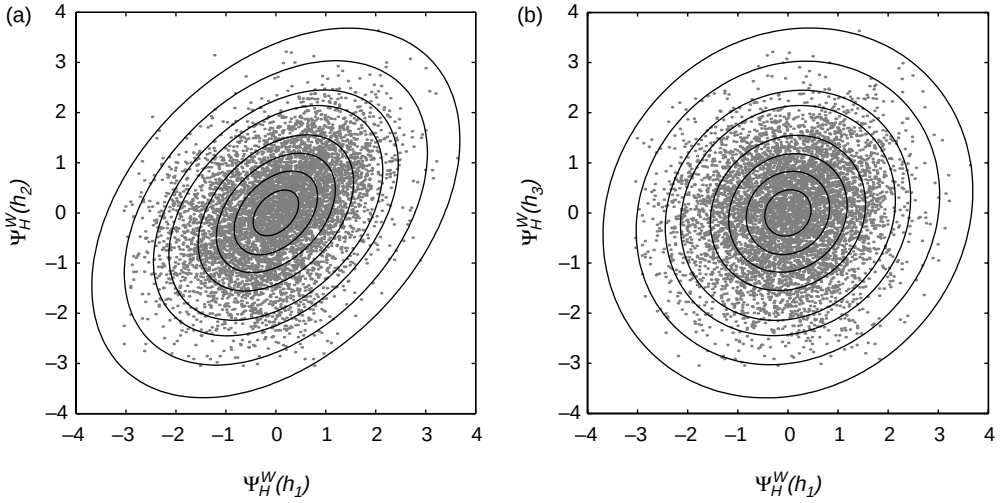

Fig. 11. Paired plot of the transformed wave height Ψ_H^W for the Draupner data between (a) h_1 and h_2, (b) h_1 and h_3, compared with a contour plot of a standard Gaussian distribution. Percent levels of the given contour lines enclosed are 10, 30, 50, 70, 90, 95, 99 and 99.9.

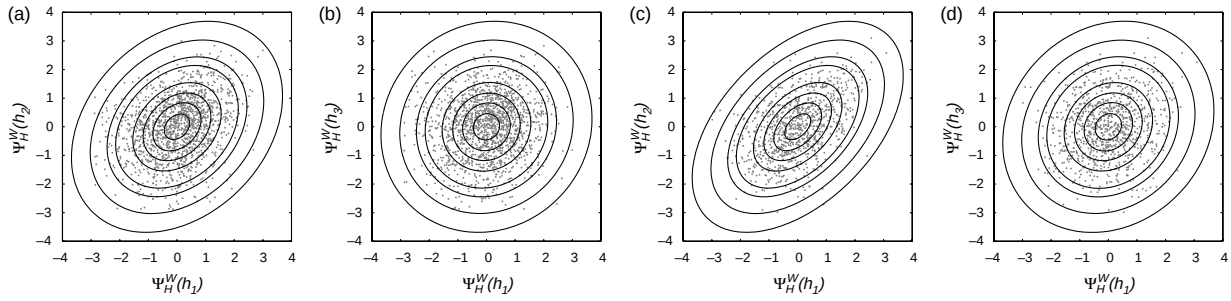

Fig. 12. Paired plot of the transformed wave height Ψ_H^{W} between (a) h_1 and h_2, (b) h_1 and h_3, for the Japan data; and between (c) h_1 and h_2, (d) h_1 and h_3 for the laboratory data, compared with a contour plot of a standard Gaussian distribution. Percent levels of the given contour lines enclosed are 10, 30, 50, 70, 90, 95, 99 and 99.9.

data are shown in Figs. 9(b) and 10(b). Overall, also for these data the Nataf–Weibull model gives the best agreement. In the following, only the Nataf–Weibull model will be considered.

Fig. 11 shows a paired plot of the transformed wave heights Ψ_H^{W} between (a) h_1 and h_2 and (b) h_1 and h_3 for the Draupner data. The solid lines are contour plots of a standard Gaussian distribution. The figure shows that the dependency structure is quite similar to the one for a standard Gaussian distribution, and thus, indicates that the transformation correctly takes care of the dependency structure. The results for the Nataf–Næss model are quite similar. Fig. 12 shows the results for the Japan data and the laboratory data, which also agree well with the standard Gaussian distribution.

The sample ACF of the transformed normalized wave heights Ψ_H^{W} from the different data sets have been calculated, and the results are shown in Fig. 13. The ACF

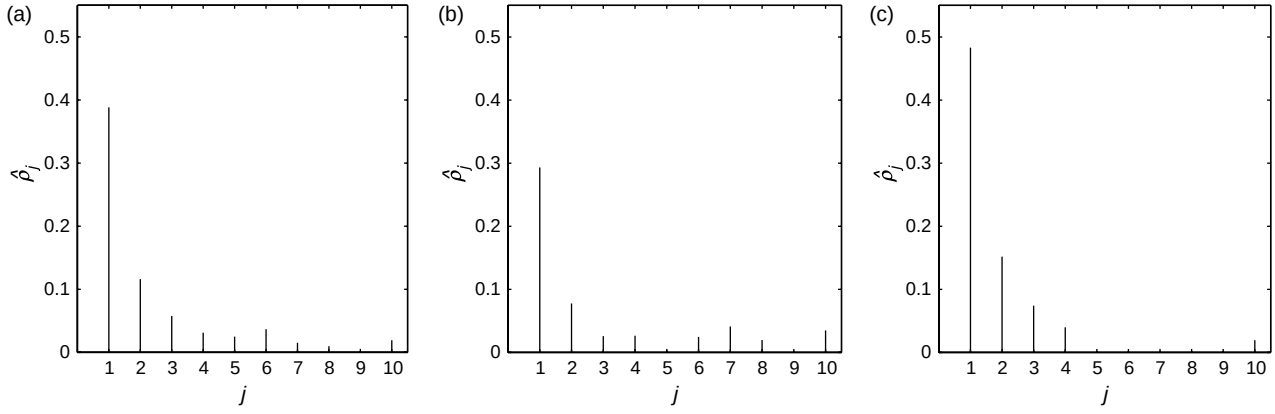

Fig. 13. Sample autocorrelation function of Ψ_H^{W} from (a) Draupner data; (b) Japan data; (c) Laboratory data.

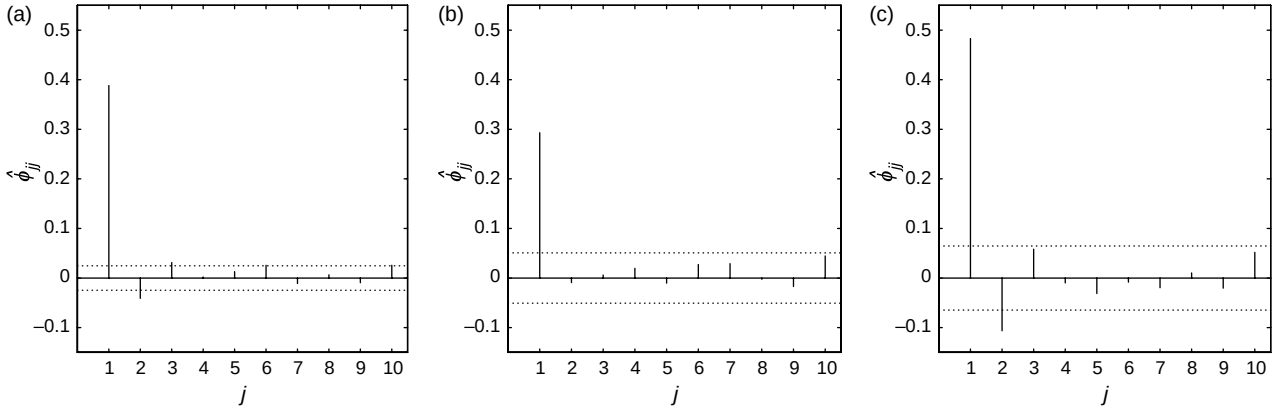

Fig. 14. Sample partial autocorrelation function of Ψ_H^{W} from (a) Draupner data; (b) Japan data; (c) Laboratory data. The dotted line indicates $\pm 2(\mathrm{Var}[\hat{\phi}_{jj}])^{1/2}$.

Table 4
Likelihood ratio test of the transformed wave heights

	Draupner data	Japan data	Lab. data
n	2189	518	319
$-2\ln\Lambda_{\text{obs}}$	6.62	6.22	3.34
Significance level (%)	3.6	4.4	18.8

decreases approximately exponentially for all cases. Fig. 14 shows the sample PACF of Ψ_H^{W} from the different data sets. The PACF has one spike at $j=1$, while the values for $j\geq 2$ are so small that they can be regarded as noise. This indicates that the process is an AR(1) process for both the field data and the laboratory data. A likelihood ratio test of the correlation coefficients of three successive wave heights following Eq. (28) resulted in an observed statistic $-2\ln\Lambda_{\text{obs}}=6.62$ for the Draupner data from a sample size of $n=2189$ triplets of wave height observations. When the sample size is large, the statistic is approximately chi-squared distributed with two degrees of freedom. From tables $\chi^2_{0.036,2}=6.65$, which means that the hypothesis would not be rejected at 3.6% significance level. The result of the likelihood ratio test is summarized in Table 4 together with the results from the Japan data and the laboratory data. This indicates that an AR(1) model is a good approximation for both the field data and the laboratory data. However, one should notice that the number of triplets from the Japan data and the laboratory data is quite small.

Simulations of transformed wave heights were made using the correlation coefficient $\rho_1=\rho_{\text{W},12}=0.388$ from the Draupner data (see Table 3). Fig. 15(a) shows the probability of exceedance of the normalized wave heights from the Draupner data and the wave heights from the simulated AR(1) model, found by Eq. (33). The two-parameter Weibull distribution and the Næss distribution [7] are included for comparison. The figure shows good agreement between the Draupner data and the simulated data from the AR(1) model.

Fig. 15(b) shows a contour plot of the two-dimensional kernel density estimate of the Draupner data and the simulated data from the AR(1) model. The simulated data compare well with the Draupner data, which indicates that the AR(1) model retains the dependency structure.

Similarily, simulations of transformated wave heights were made using the correlation coefficient $\rho_1=\rho_{W,12}$ from the Japan data and the laboratory data given in Table 3. The results are given in Fig. 16. The simulated data from the AR(1) model agree quite well with the field data and the laboratory data.

Fig. 17 shows the Nataf–Weibull model in Eq. (21) in terms of probability of exceedance for $p=1, 2, 3$. The three-dimensional distribution based on the AR(1) model (Eq. (34)) is also included. The results are compared with data from the Draupner field. From the figure it is clear that the probability of p successive wave heights exceeding a value h decreases when p increases. The Nataf–Weibull model agrees quite well with the data for all values of p shown in the figure. The three-dimensional Nataf–Weibull model and the three-dimensional distribution based on the AR(1) model are almost identical.

The corresponding results for the Japan data and the laboratory data are shown in Fig. 18(a) and (b), respectively. The figures show similar results as for the Draupner data. One should note that the length of the time series of the laboratory data is quite short in order to make a reliable three-dimensional kernel density estimate. However, the result is included for comparison.

By using the Nataf transformation, the probability distribution for two and three successive wave heights can be modeled by a transformed multivariate Gaussian distribution. The transformed Gaussian distribution can also be applied for more than three successive wave heights,

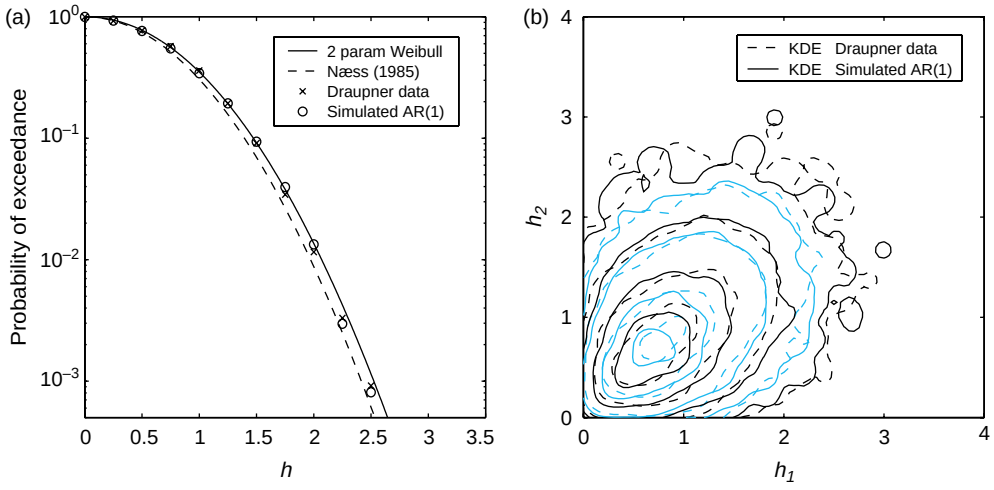

Fig. 15. (a) Probability of exceedance of normalized wave heights, and (b) contour plot of the two-dimensional kernel density estimates for the Draupner data. Percent levels of the given contour lines enclosed are 10, 30, 50, 70, 90, 95, 99 and 99.9.

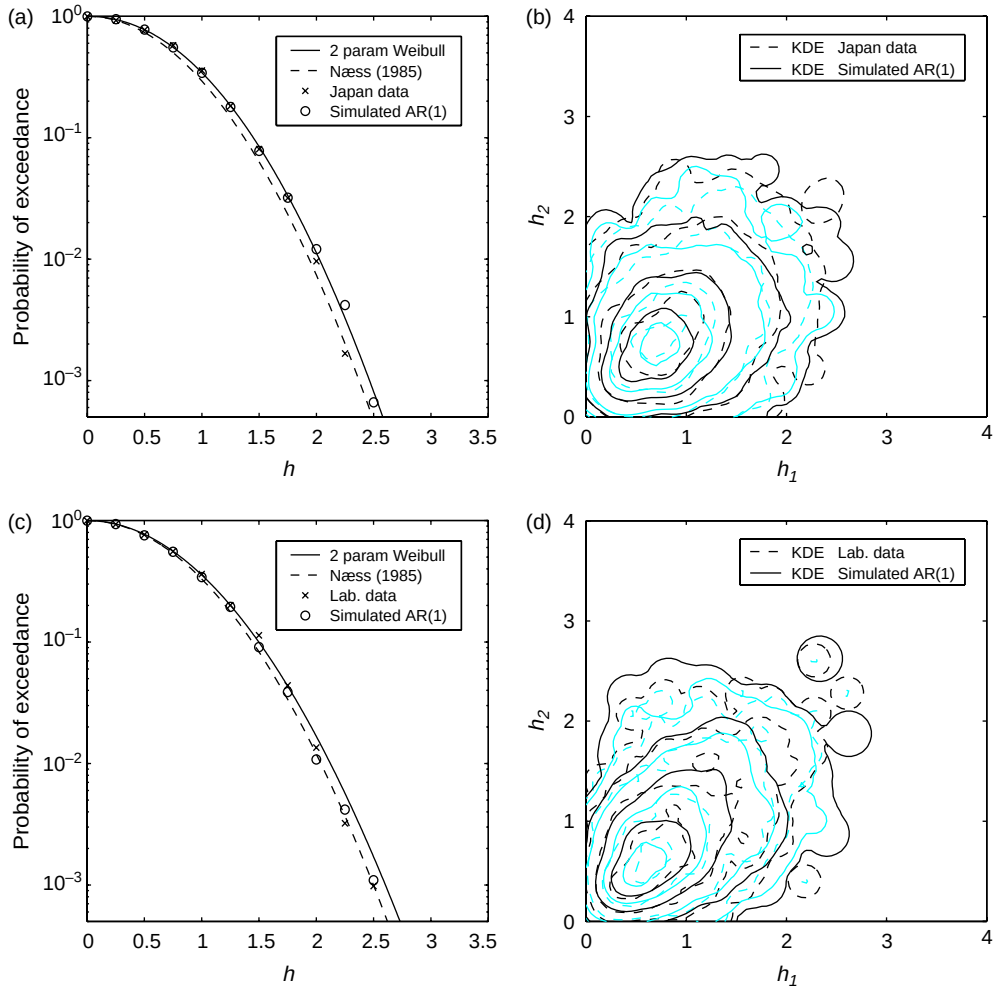

Fig. 16. Probability of exceedance of normalized wave heights for (a) Japan data; (c) Laboratory data. Contour plot of the two-dimensional kernel density estimates for (b) Japan data; (d) Laboratory data. Percent levels of the given contour lines enclosed are 10, 30, 50, 70, 90, 95, 99 and 99.9.

but then the dependency structure should be further examined by, e.g. paired plots.

The process of successive wave heights can be approximated by an AR(1) model. This gives two favorable results. First, the model has the Markov property, which means that only a two-dimensional distribution is needed when calculating the conditional statistical properties. Joint distributions can then be constructed by combining bivariate conditional distributions, as exemplified in Eq. (34) for the three-dimensional distribution. Second, the simulation of successive wave heights can be done from Eqs. (31) and (33) (or Eq. (32)). This is a simple and fast method, if the time series of the complete surface elevation is not required.

4.3. Successive wave periods for large wave heights

First, results will be shown to justify the approximation of an AR(1) model to the process of transformed successive wave periods. The sample ACF of the transformed normalized wave periods Ψ_T^G from the different data sets have been calculated, and the results are shown in Fig. 19. The ACF

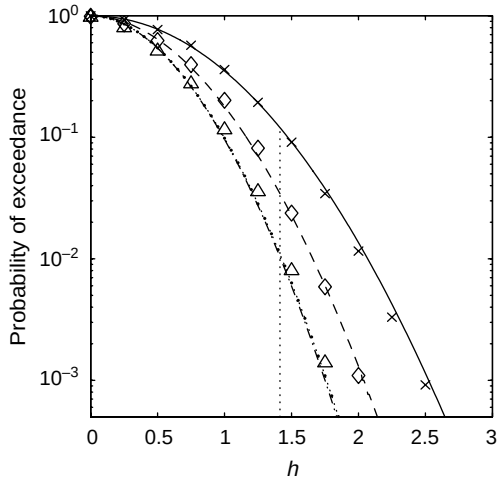

Fig. 17. Probability of exceedance for normalized wave heights for the Draupner data. $P(H_1>h)$: — Nataf–Weibull model; × data; $P(H_1>h, H_2>h)$: – – Nataf–Weibull model; ◇ data; $P(H_1>h, H_2>h, H_3>h)$: –·– Nataf–Weibull model; ··•·· AR(1) model; △ data. The dotted line indicates the normalized significant wave height of $\sqrt{2}$.

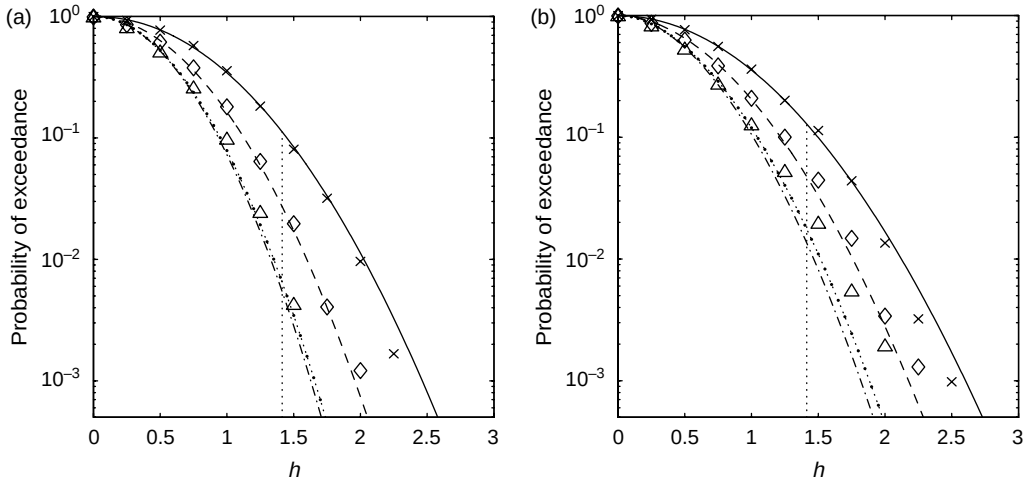

Fig. 18. Probability of exceedance for normalized wave heights for (a) Japan data, (b) Laboratory data. $P(H_1 > h)$: —Nataf–Weibull model; × data; $P(H_1 > h, H_2 > h)$: – – Nataf–Weibull model; ◇ data; $P(H_1 > h, H_2 > h, H_3 > h)$: –·– Nataf–Weibull model; ··•·· AR(1) model; △ data. The dotted line indicates the normalized significant wave height of $\sqrt{2}$.

decreases approximately exponentially for all cases. Fig. 20 shows the sample PACF of Ψ_T^G from the different data sets. The PACF has one spike at $j=1$, while the values for $j \geq 2$ are so small that they can be regarded as noise.

The results of the likelihood ratio test of the correlation coefficients of three successive wave periods following Eq. (28) are given in Table 5. However, one should notice that the number of triplets from the Japan data and

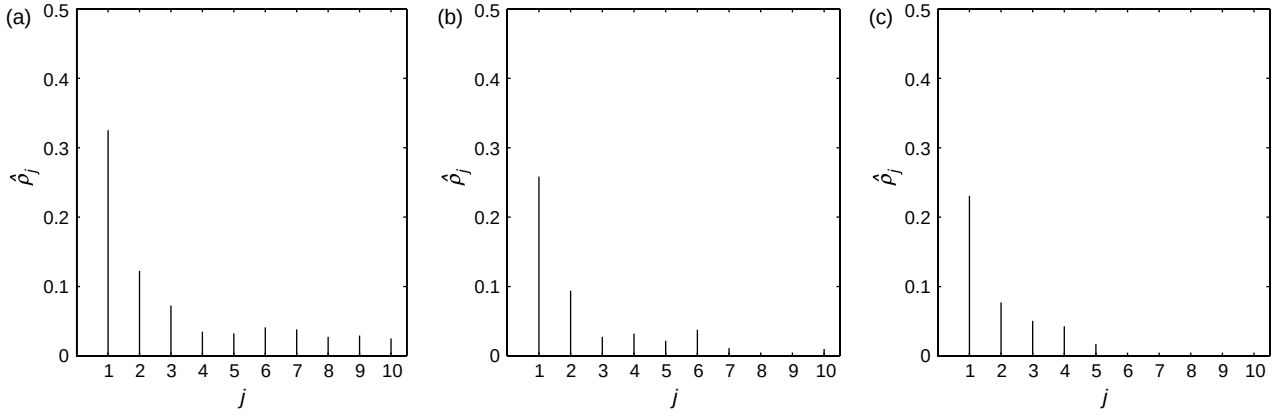

Fig. 19. Sample autocorrelation function of Ψ_T^G from (a) Draupner data; (b) Japan data; (c) Laboratory data.

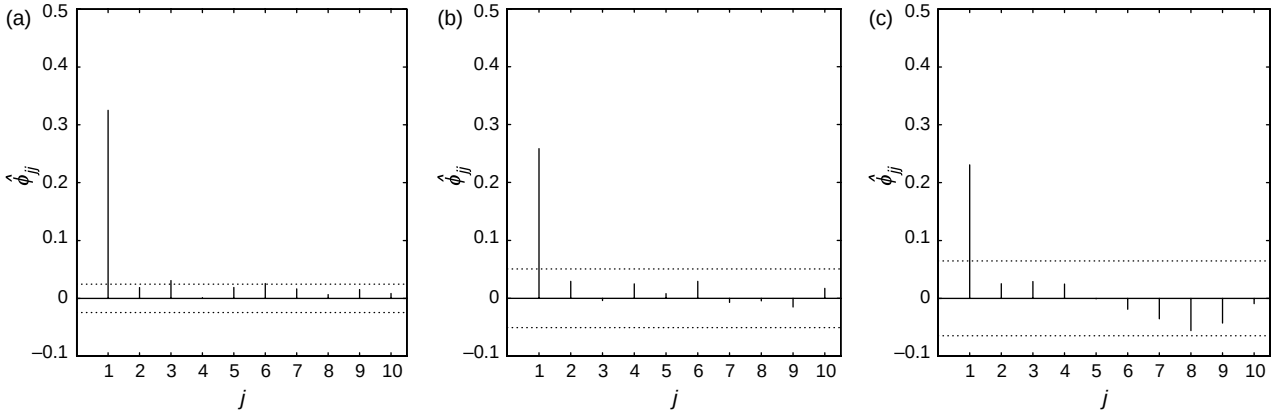

Fig. 20. Sample partial autocorrelation function of Ψ_T^G from (a) Draupner data; (b) Japan data; (c) Laboratory data. The dotted line indicates $\pm 2(\mathrm{Var}[\hat{\phi}_{jj}])^{1/2}$.

Table 5
Likelihood ratio test of the transformed wave periods

	Draupner data	Japan data	Lab. data
n	2208	521	319
$-2\ln\Lambda_{\text{obs}}$	3.17	1.65	6.38
Significance level (%)	20.5	43.7	4.1

the laboratory data is quite small. The likelihood ratio test together with Figs. 19 and 20 indicate that an AR(1) model is a good approximation for both the field data and the laboratory data. This means that the Markov property in Eq. (30) applies for all wave periods, and thus, for the wave periods where the corresponding wave heights are larger than a given threshold, e.g. larger than h_{rms}. Consequently, the distribution for the wave period given the previous wave period will be independent of the wave periods prior to the previous wave period, also when considering wave periods with corresponding large wave heights.

Next, only wave periods with corresponding wave heights exceeding a given threshold will be considered.

Fig. 21(a) shows a histogram of the normalized wave periods from the Draupner data where the corresponding normalized wave height is larger than $h_{\text{rms}}=1$, and the kernel density estimate of the data. The data are compared with the Longuest-Higgins models [14,15] (Eqs. (46) and (47)) and the Tayfun model [17] (Eq. (49)). The first two models do not give a good prediction of the wave periods. The density functions are shifted towards lower values of t, and the peak value is also underestimated. The latter model gives a better estimate of the wave periods. However, this model also underestimates the peak value of the kernel density function.

The shape of the data in Fig. 21(a) indicates that a Gaussian density function would give a good description of the data. Fig. 21(b) shows the data compared with a Gaussian density function with mean value and standard deviation calculated from the data, which are given in Table 6 for $p=1$. The Gaussian density function agrees well with the data.

The histograms and kernel density estimates of the normalized wave periods from the Japan data and the laboratory data where the corresponding normalized wave height is larger than $h_{\text{rms}}=1$ are shown in Fig. 22(a) and (b), respectively. A Gaussian pdf with mean value and standard deviation given in Table 6 for $p=1$ is also included. The figures show that the Gaussian pdf agree well with the data, while the other densities do not give a good estimation of the data.

In order to compare the multivariate theory with the data, pairs and triplets of successive wave periods were formed conditioned on that the corresponding wave height was larger than $h_{\text{rms}}=1$. The mean value and standard deviation are shown in Table 6 for $p=2$ and 3, respectively, and n is the number of pairs and triplets that were found. In addition, the correlation coefficients, $\boldsymbol{\rho}=[\rho_{12},\ldots,\rho_{1p}]^{\text{T}}$, between

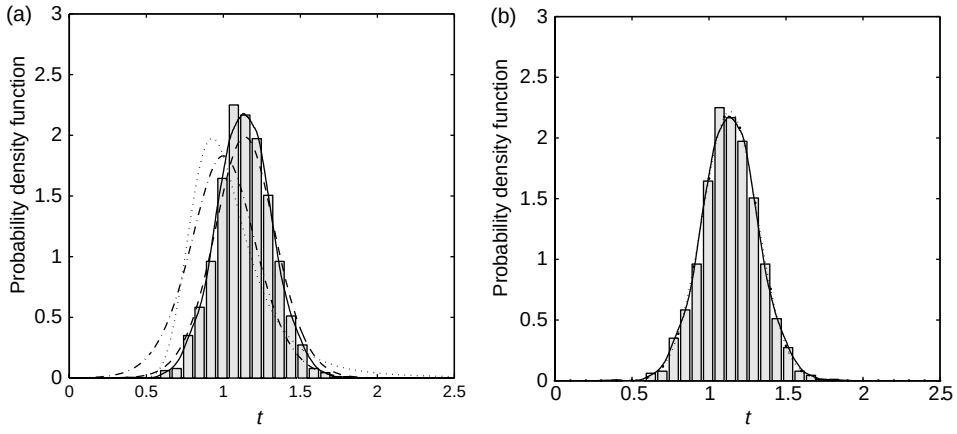

Fig. 21. Pdf of wave periods where the corresponding wave height is larger than h_{rms}, i.e. $h>1$; (a) — kernel density estimate of Draupner data, –·– [14], ··· [15], – – [17]. (b) — kernel density estimate of Draupner data, ··•·· Gaussian density function ($\mu_{t|\tilde{h}}=1.14$, $\sigma_{t|\tilde{h}}=0.18$).

Table 6
Calculated parameters for the p-dimensional Gaussian distribution with $\tilde{h}=1$

		$\boldsymbol{\mu}_{t\|\tilde{h}}$	$\boldsymbol{\sigma}_{t\|\tilde{h}}$	$\boldsymbol{\rho}$	n
Draupner	$p=1$	1.14	0.18		2424
	$p=2$	$[1.18, 1.19]^{\text{T}}$	$[0.17, 0.17]^{\text{T}}$	0.245	1360
	$p=3$	$[1.18, 1.23, 1.19]^{\text{T}}$	$[0.17, 0.16, 0.16]^{\text{T}}$	$[0.287, 0.150]^{\text{T}}$	768
Japan	$p=1$	1.15	0.18		555
	$p=2$	$[1.21, 1.19]^{\text{T}}$	$[0.16, 0.17]^{\text{T}}$	0.091	279
	$p=3$	$[1.19, 1.24, 1.18]^{\text{T}}$	$[0.16, 0.14, 0.17]^{\text{T}}$	$[0.143, -0.050]^{\text{T}}$	149
Lab.	$p=1$	1.05	0.11		347
	$p=2$	$[1.09, 1.08]^{\text{T}}$	$[0.09, 0.09]^{\text{T}}$	−0.052	201
	$p=3$	$[1.08, 1.10, 1.08]^{\text{T}}$	$[0.08, 0.08, 0.10]^{\text{T}}$	$[0, -0.027]^{\text{T}}$	116

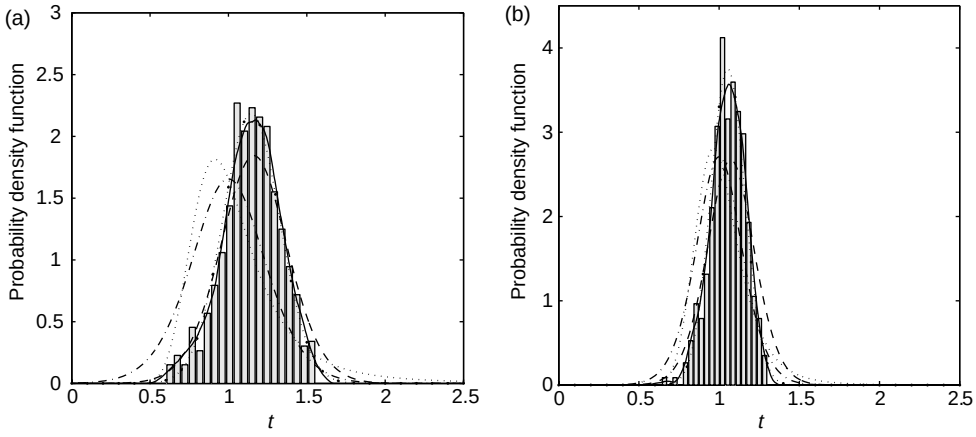

Fig. 22. Pdf of wave periods where the corresponding wave height is larger than h_{rms}, i.e. $h>1$; — kernel density estimate of data, –·– [14], ··· [15], – – [17]. ··●·· Gaussian density function (a) Japan data; (b) Laboratory data.

the successive wave periods are given. If the normalized significant wave height of $\sqrt{2}$ was selected as $\tilde{h}$, the number n would be much smaller. One should note that the number of data cases available for $p=2$ and 3 is small for both the Japan data and the laboratory data, but they are included for comparison.

Fig. 23(a) shows a contour plot of the bivariate Gaussian distribution in Eq. (52) with $p=2$ and $\tilde{h}=1$, compared with

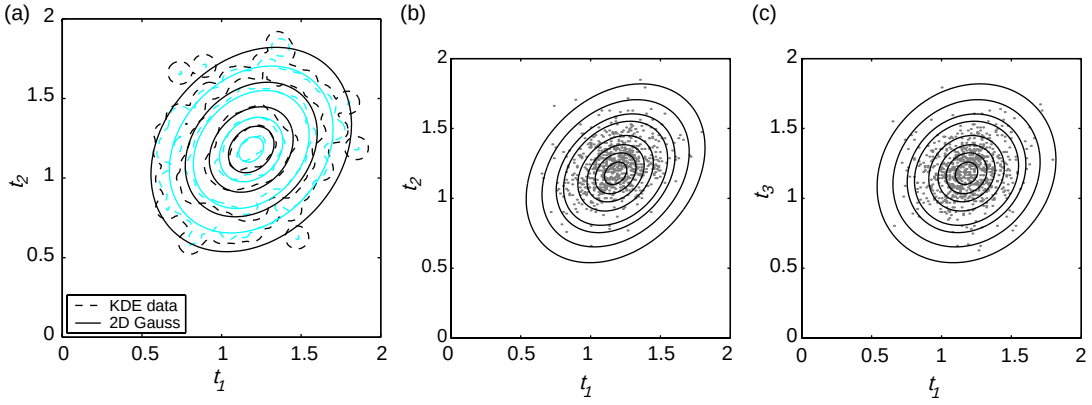

Fig. 23. (a) Contour plot of two successive wave periods, given that the corresponding wave heights are larger than $h_{\text{rms}}=1$, modeled by the bivariate Gaussian probability density function and compared with kernel density estimate of Draupner data. Percent levels of the given contour lines enclosed are 10, 30, 50, 70, 90, 95, 99 and 99.9. Paired plot between (b) t_1 and t_2, and (c) t_1 and t_3.

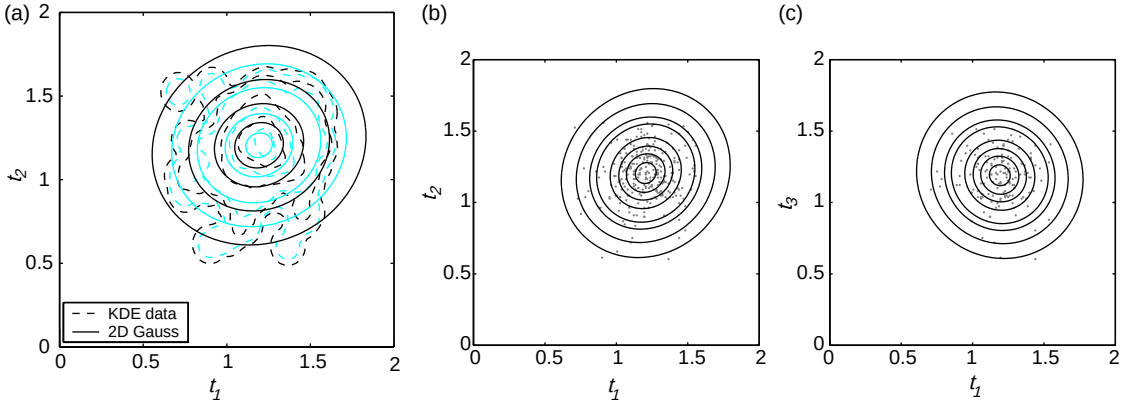

Fig. 24. (a) Contour plot of two successive wave periods, given that the corresponding wave heights are larger than $h_{\text{rms}}=1$, modeled by the bivariate Gaussian probability density function and compared with kernel density estimate of Japan data. Percent levels of the given contour lines enclosed are 10, 30, 50, 70, 90, 95, 99 and 99.9. Paired plot between (b) t_1 and t_2, and (c) t_1 and t_3.

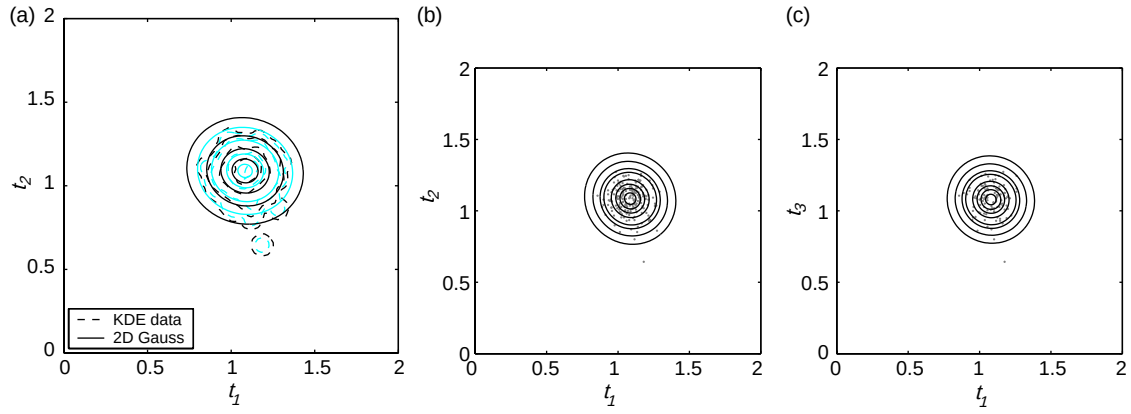

Fig. 25. (a) Contour plot of two successive wave periods, given that the corresponding wave heights are larger than $h_{\text{rms}} = 1$, modeled by the bivariate Gaussian probability density function and compared with kernel density estimate of Laboratory data. Percent levels of the given contour lines enclosed are 10, 30, 50, 70, 90, 95, 99 and 99.9. Paired plot between (b) t_1 and t_2, and (c) t_1 and t_3.

the kernel density estimate of the Draupner data. The figure shows fairly good correspondence between the model and the data. In order to verify that the multivariate Gaussian distribution can be used for modeling successive wave periods, the dependency structure should be examined. Fig. 23(b) and (c) show a paired plot of the wave periods t_1 and t_2, and t_1 and t_3, respectively. The figure shows that the correlation structure is correctly modeled by the bivariate Gaussian distribution.

The corresponding results for the Japan data and the laboratory data are shown in Figs. 24 and 25, respectively. Note that the outer contour lines of the kernel density estimates are based on very few data points. The behavior around the peak value of the kernel density estimates, where most of the data are located, are well described by the bivariate Gaussian distribution.

Thus, the probability distribution for two and three successive wave periods given that the corresponding wave heights exceeded a critical level, e.g. h_{rms}, can be modeled by a multivariate Gaussian distribution. The multivariate Gaussian distribution can also be applied for more than three wave periods with corresponding large wave heights, but then the dependency structure should be further examined.

When estimating, e.g. resonance phenomena, a quantity of interest is the probability that a wave period is in an interval $[\tilde{t}_1, \tilde{t}_2]$ given that the previous wave period was in the same interval. This has been studied in, e.g. [27], as marine systems often are exposed to such waves. However, dangerous situations occur in high waves, so the quantity of interest should be conditioned on the corresponding wave heights exceeding a given threshold. Thus, the present results should represent a useful tool to assess the probability of occurrence of resonance phenomena at sea.

Fig. 26(a) shows the probability that a wave period is in an interval $[\tilde{t}_1, \tilde{t}_2]$ given that the previous wave period was in the same interval, and given that the two corresponding wave heights exceeded h_{rms}. This is shown as a function of $x = (\tilde{t}_1 + \tilde{t}_2)/2$. Here $\tilde{t}_1 = x - 0.1$ and $\tilde{t}_2 = x + 0.1$.

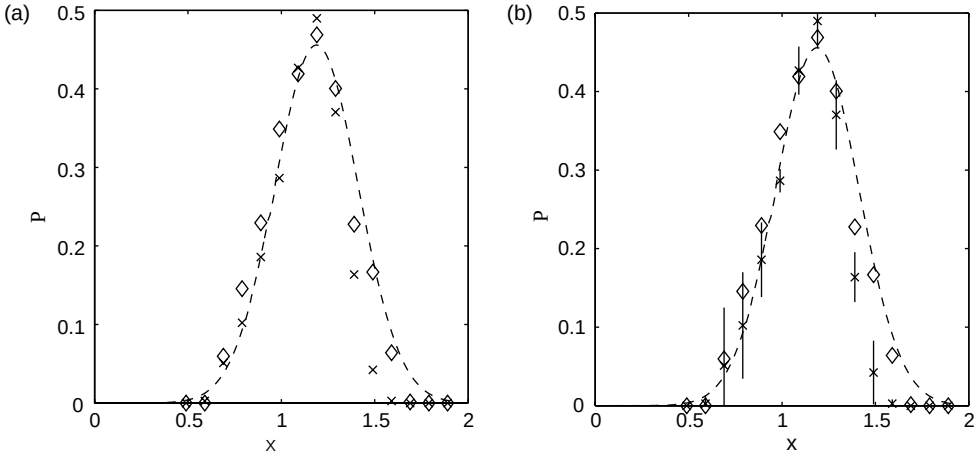

Fig. 26. The probability that a wave period is in an interval $[\tilde{t}_1, \tilde{t}_2]$ given that the previous wave period was in the same interval, where $\tilde{t}_1 = x - 0.1$ and $\tilde{t}_2 = x + 0.1$, and given that the two corresponding wave heights exceeded h_{rms}. – – Gaussian model; ◇ Draupner data; × simulated data. (a) Data and mean values of simulations. (b) Simulations including confidence intervals. ($P = P(\tilde{t}_1 < T_2 < \tilde{t}_2 | \tilde{t}_1 < T_1 < \tilde{t}_2, H_1 > 1, H_2 > 1)$).

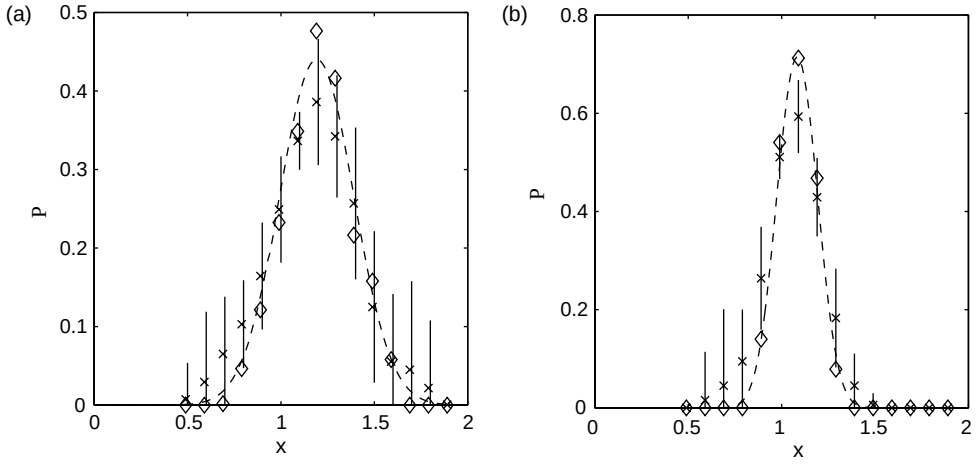

Fig. 27. The probability that a wave period is in an interval $[\tilde{t}_1, \tilde{t}_2]$ given that the previous wave period was in the same interval, where $\tilde{t}_1 = x - 0.1$ and $\tilde{t}_2 = x + 0.1$, and given that the two corresponding wave heights exceeded h_{rms}. – – Gaussian model; ◇ data; × mean values of simulated data with confidence intervals. (a) Japan data. (b) Laboratory data. ($P = P(\tilde{t}_1 < T_2 < \tilde{t}_2 | \tilde{t}_1 < T_1 < \tilde{t}_2, H_1 > 1, H_2 > 1)$).

Simulated data and field data from the Draupner field are included, and the model agrees quite well with the data except for larger values of x for the simulated data. The simulated data show fairly good agreement with the field data. Fig. 26(b) shows the variation in the simulated data, where the confidence intervals are given by $\pm 2\text{Var}[y]^{1/2}$, where y is a vector of the 10 simulation points. The confidence intervals cover the field data for most of the smaller values of x, but there is larger difference between the field data and the simulations for large values of x.

Fig. 27(a) and (b) show the results for the Japan data and the laboratory data, respectively. The Gaussian model agrees well with the field data and the laboratory data. Here, the field data and laboratory data have a larger peak than the simulated data. However, due to the large variation in the simulated data, the confidence intervals cover the field data and the laboratory data, as well as the Gaussian model, for almost all values of x.

Fig. 28 shows the probability of a wave period being in an interval $[\tilde{t}_1, \tilde{t}_2]$ given that the two previous wave periods were in the same interval, as a function of $x = (\tilde{t}_1 + \tilde{t}_2)/2$. All corresponding wave heights exceed h_{rms}. The results are quite similar to the results in Figs. 26 and 27. This supports the hypothesis that the process of successive wave periods can be approximated by an AR(1) model. Then it follows from the Markov property that

$$f_{T_3|T_2,T_1,H_3,H_2,H_1}(t_3|t_2,t_1,\ h_3>1,h_2>1,h_1>1) = f_{T_3|T_2,H_3,H_2}(t_3|t_2,h_3>1,h_2>1). \quad (54)$$

Thus, joint distributions of successive wave periods with large wave heights can be constructed by combining bivariate conditional distributions, similarly to Eq. (45). The conditional density functions are given similarly as for the wave heights in Eq. (35), where the joint pdf and marginal pdf are given in Eq. (52) with $p = 2$ and 1, respectively.

For practical purposes, it is of more interest to study the wave periods for wave heights exceeding the significant wave height. The calculated parameters from the Draupner

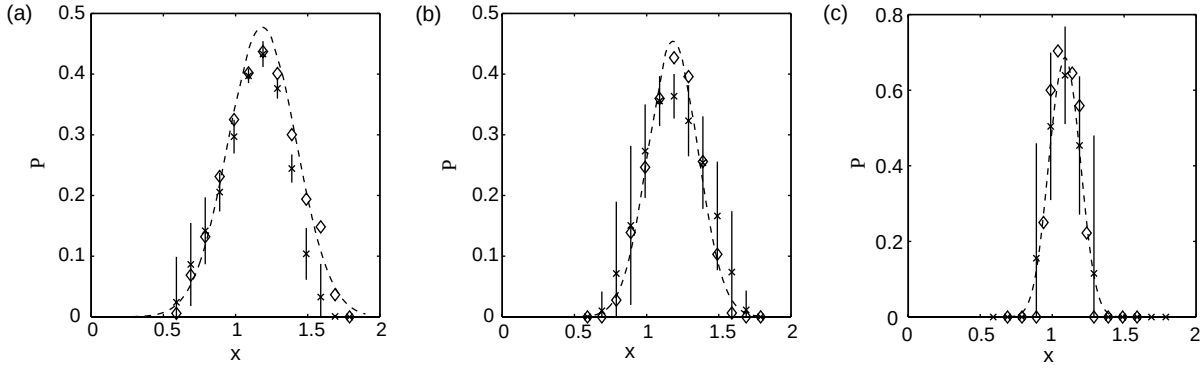

Fig. 28. The probability that a wave period is in an interval $[\tilde{t}_1, \tilde{t}_2]$ given that the two previous wave periods were in the same interval, where $\tilde{t}_1 = x - 0.1$ and $\tilde{t}_2 = x + 0.1$, and given that the three corresponding wave heights exceeded h_{rms}. – – Gaussian model; ◇ data; × mean values of simulated data with confidence intervals. (a) Draupner data. (b) Japan data. (c) Laboratory data. ($P = P(\tilde{t}_1 < T_3 < \tilde{t}_2 | \tilde{t}_1 < T_2 < \tilde{t}_2, \tilde{t}_1 < T_1 < \tilde{t}_2, H_1 > 1, H_2 > 1, H_3 > 1)$).

Table 7
Calculated parameters for the p-dimensional Gaussian distribution with $\tilde{h} = \sqrt{2}$ (normalized value of H_{m0}), from the Draupner field data

	$\boldsymbol{\mu}_{t\|\tilde{h}}$	$\boldsymbol{\sigma}_{t\|\tilde{h}}$	$\boldsymbol{\rho}$	n
$p=1$	1.15	0.15		798
$p=2$	$[1.21, 1.21]^{\mathrm{T}}$	$[0.15, 0.13]^{\mathrm{T}}$	0.217	251
$p=3$	$[1.20, 1.26, 1.21]^{\mathrm{T}}$	$[0.15, 0.14, 0.11]^{\mathrm{T}}$	$[0.361, 0.196]^{\mathrm{T}}$	80

field data when constructing pairs and triplets of wave periods conditioned on the corresponding wave heights exceeding H_{m0} are shown in Table 7. Compared to the values in Table 6, where the corresponding wave heights exceeded h_{rms}, the difference in the parameters for the Gaussian distribution is small, but the number n has decreased significantly. Thus, in order to compare with data, especially if two or three successive wave periods are considered, a long time series is needed, as mentioned earlier. When considering three successive waves with corresponding wave heights exceeding H_{m0}, the time series of the Draupner field data, which was nearly 16 h, only resulted in 80 data cases. The corresponding numbers of data cases for three successive wave periods for the Japan data and the laboratory data are too small; thus these data are not included in the analysis.

Fig. 29(a) shows the probability that a wave period is in an interval $[\tilde{t}_1, \tilde{t}_2]$ of size 0.2 given that the previous wave period were in the same interval, and given that the two corresponding wave heights exceeded the normalized value of H_{m0}, i.e. $\sqrt{2}$. The results show fairly good agreement between the Draupner data and the model. The confidence intervals of the simulations are included in (b). The confidence intervals cover the field data for smaller values of x, but there is larger difference between the field data and the simulations for large values of x.

5. Conclusions

The existing wave height models are applicable when modeling only two successive wave heights. In this paper a Gaussian copula, which is often referred to as the Nataf model, is used for modeling three successive wave heights. The difficulty is to find the initial distribution for which the transformation is approximately Gaussian. Both the Næss model [7] and a two-parameter Weibull distribution have been used in the transformation, where the latter was in best agreement with the data. However, the parameters in the Weibull distribution must be estimated for each data set. The transformed multivariate Gaussian distribution can in theory be applied for modeling more than three successive wave heights, but then the dependency structure should be examined in order to validate that the correlation between the wave heights is correctly taken care of during the transformation. The results show that the Nataf model is more sensitive to variation in the data set than the existing models. Thus, the parameter estimation is crucial for the behavior of the distribution.

Results have shown that the Nataf transformation of successive wave heights can be approximated by a first order autoregressive model. This gives two major advantages. First, the time series has the Markov property, i.e. the distribution of the wave height given the previous wave height is independent of the wave heights prior to the previous wave height. Joint distributions can then be constructed by combining bivariate conditional distributions. Second, the simulation of successive wave heights can be done directly by simulating a series of transformed wave heights and then find the wave heights by inverting the transformation. This is a simple and fast simulation technique, which is useful when the time series of the complete surface elevation is not needed.

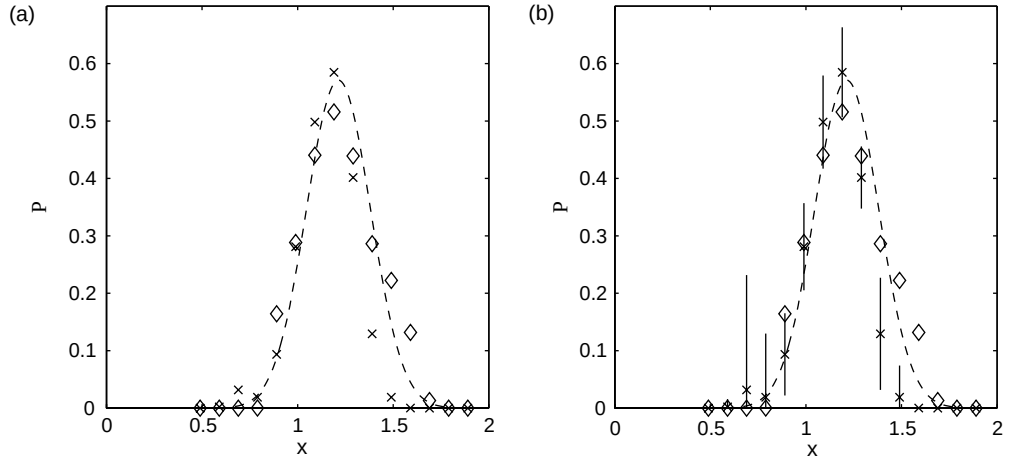

Fig. 29. The probability that a wave period is in an interval $[\tilde{t}_1, \tilde{t}_2]$ given that the previous wave period was in the same interval, where $\tilde{t}_1 = x - 0.1$ and $\tilde{t}_2 = x + 0.1$, and given that the two corresponding wave heights exceeded H_{m0}. – – Gaussian model; ◇ Draupner data; × simulated data. (a) Data and mean values of simulations. (b) Simulations including confidence intervals ($P = P(\tilde{t}_1 < T_2 < \tilde{t}_2 | \tilde{t}_1 < T_1 < \tilde{t}_2, H_1 > \sqrt{2}, H_2 > \sqrt{2})$).

Several models exist for modeling a single wave period. None of them capture the shape of the pdf of the data, but the Bretschneider model [13] agrees quite well with the data for large wave periods. The Nataf transformation can also be used when modeling more than two successive wave periods. The shape of the pdf of the data, however, makes it difficult to select an initial distribution so that the transformation is approximately Gaussian. A generalized Gamma distribution has been used here as initial distribution. The model gives satisfactory results compared with the existing models.

When considering successive wave periods for large waves, the pdf for the wave periods can be approximated by a Gaussian density function. This means that a transformation is not necessary, and three successive wave periods with corresponding large wave heights can be modeled by the three-dimensional Gaussian distribution. The multivariate Gaussian distribution can also be applied for more than three wave periods with corresponding large wave heights, but then the dependency structure should be further examined. When comparing with data, the number of data cases decreases rapidly both if the selected level of the corresponding wave height increases and if the number of successive periods of interest increases. Thus, a long time series is needed in order to obtain enough data cases.

Acknowledgements

This study was financially supported by the Norwegian Research Council (NFR). The wave data from Draupner was prepared and made available by Dr Sverre Haver, Statoil. The wave data from the Japan Sea was prepared and made available by the National Maritime Research Institute, Mitaka, Tokyo. The laboratory data from HR Wallingford was collected during experimental studies carried out with financial support from the European Union under the TMR programme.

References

[1] Longuet-Higgins MS. On the statistical distribution of the heights of sea waves. J Mar Res 1952;11(3):245–66.
[2] Cartwright DE, Longuet-Higgins MS. The statistical distribution of the maxima of a random function. Proc R Soc London, Ser A 1956; 237:212–32.
[3] Prevosto M, Forristall GZ. Statistics of wave crests from models vs. measurements. In: Proceedings of OMAE'02, 21st international conference on offshore mechanics and arctic engineering, Oslo, Norway, OMAE2002-28443; 2002.
[4] Wist HT, Myrhaug D, Rue H. Joint distributions of successive wave crest heights and successive wave trough depths for second-order nonlinear waves. J Ship Res 2002;46(3):175–85.
[5] Wist HT. Statistical properties of successive ocean wave parameters. Dr.ing. Thesis, Norwegian University of Science and Technology, Faculty of Engineering Science and Technology, Trondheim, Norway.
[6] Longuet-Higgins MS. On the distribution of the heights of sea waves: some effects of nonlinearity and finite band width. J Geophys Res 1980;85(C3):1519–23.
[7] Næss A. On the distribution of crest to trough wave heights. Ocean Eng 1985;12(3):221–34.
[8] Vinje T. The statistical distribution of wave heights in a random seaway. Appl Ocean Res 1989;11(3):143–52.
[9] Kimura A. Statistical properties of random wave groups, vol. III. In: Proceedings of the 17th coastal engineering conference. ASCE, Sydney, Australia; 1980. p. 2955–73.
[10] Myrhaug D, Dahle EA, Rue H. A two-dimensional Weibull distribution and its application to rolling. J Offshore Mech Arctic Eng 1995;117(3):178–82.
[11] Nataf A. Détermination des distributions de probabilités dont les marges sont données. Comptes Rendus Hebdomadaires des Séances de l'Académie des Sciences 1962;255:42–3.
[12] France WN, Levadou M, Trakle TW, Paulling JR, Michel RK, Moore C. An investigation of head-sea parametric rolling and its influence on container lashing systems. Mar Technol 2003;40(1): 1–19.
[13] Bretschneider CL. Wave variability and wave spectra for wind-generated gravity waves. Beach Erosion Board, US Army Corps of Engineers. Technical Memorandum 118; 1959.
[14] Longuet-Higgins MS. On the joint distribution of the periods and amplitudes of sea waves. J Geophys Res 1975;80(18):2688–94.
[15] Longuet-Higgins MS. On the joint distribution of wave periods and amplitudes in a random wave field. Proc R Soc London, Ser A 1983; 389:241–58.
[16] Cavanié A, Arhan M, Ezraty R. A statistical relationship between individual heights and periods of storm waves, vol. 2. In: Proceedings of the first international conference on behaviour of off-shore structures, Trondheim, Norway; 1976. p. 354–60.
[17] Tayfun MA. Joint distributions of large wave heights and associated periods. J Waterway, Port, Coastal, Ocean Eng 1993;119(3):261–73.
[18] Lindgren G, Rychlik I. Wave characteristic distributions for Gaussian waves—wave-length, amplitude and steepness. Ocean Eng 1982;9(5): 411–32.
[19] Rychlik I, Johannesson P, Leadbetter MR. Modelling and statistical analysis of ocean-wave data using transformed Gaussian process. Mar Struct 1997;10:13–47.
[20] Guedes Soares C. Representation of double-peaked sea wave spectra. Ocean Eng 1984;11:185–207.
[21] Rodríguez GR, Guedes Soares C, Pacheco M, Pérez-Martell E. Wave height distribution in mixed sea states. J Offshore Mech Arctic Eng 2002;124:34–40.
[22] Rodríguez GR, Guedes Soares C. Wave period distribution in mixed sea states. In: Proceedings of ETCE/OMAE2000 joint conference energy for the new millenium, New Orleans, Louisiana, OMAE2000/S&R-6132; 2000.
[23] Rodríguez GR, Guedes Soares C. The bivariate distribution of wave heights and periods in mixed sea states. J Offshore Mech Arctic Eng 1999;121:102–8.
[24] Rodríguez GR, Guedes Soares C. Correlation between successive wave heights and periods in mixed sea states. Ocean Eng 2001;28: 1009–30.
[25] Myrhaug D, Rue H. Note on a joint distribution of successive wave periods. J Ship Res 1993;37(3):208–12.
[26] Myrhaug D, Rue H. Joint distribution of successive wave periods revisited. J Ship Res 1998;42(3):199–206.
[27] Myrhaug D, Slaattelid OH. Statistical properties of successive wave periods. J Offshore Mech Arctic Eng 1999;121:166–71.
[28] Myrhaug D, Dahle EA, Rue H, Slaattelid OH. Statistics of successive wave periods with application to rolling of ships. Int Shipbuilding Prog: Mar Technol Quarterly 2000;47(451):253–66.
[29] Goda Y. Estimation of wave statistics from spectral information, vol. 1. In: Proceedings of the international symposium on ocean wave

measurement and analysis. ASCE, New Orleans, Louisiana; 1974. p. 320–37.
[30] Haring RE, Osborne AR, Spencer LP. Extreme wave parameters based on continental shelf storm wave records. In: Proceedings of the 15th coastal engineering conference, Honolulu, Hawaii; 1976. p. 151–70.
[31] Forristall GZ. On the statistical distribution of wave heights in a storm. J Geophys Res 1978;83(C5):2353–8.
[32] Boccotti P. Relations between characteristic sea wave parameters. J Geophys Res 1982;87(C6):4267–8.
[33] Longuet-Higgins MS. Wave group statistics. In: Monahan EC, Mac Niocaill G, editors. Oceanic whitecaps. Dordrecht: D. Reidel; 1986. p. 15–35.
[34] Nelsen RB. An introduction to copulas. Lecture notes in statistics. vol. 139. New York: Springer; 1999.
[35] Schweizer B. Thirty years of copulas. In: Advances in probability distributions with given marginals, Rome, Italy; 1991. p. 13–50.
[36] Fréchet M. Les tableaux de corrélation et les programmes linéaires. Revue de l'Institut international de statistique 1957;25:23–40.
[37] Liu P-L, Der Kiureghian A. Multivariate distribution models with prescribed marginals and covariances. Probab Eng Mech 1986;1(2): 105–12.
[38] Monbet V, Prevosto M. Bivariate simulation of non stationary and non Gaussian observed processes. Application to sea state parameters. Appl Ocean Res 2001;23(3):139–45.
[39] Fouques S, Myrhaug D, Nielsen FG. Seasonal modelling of multivariate distributions of metocean parameters with application to marine operations. J Offshore Mech Arctic Eng 2004;126(3): 202–12.
[40] Wei WWS. Time series analysis: univariate and multivariate methods. Redwood City, CA: Addison-Wesley; 1990.
[41] Sobey RJ. Correlation between individual waves in a real sea state. Coastal Eng 1996;27:223–42.
[42] Johnson RA, Wichern DW. Applied multivariate statistical analysis. 3rd ed. Englewood cliffs, NJ: Prentice-Hall; 1992.
[43] Ochi MK. New approach for estimating the severest sea state from statistical data, vol. 1. In: Coastal engineering 1992: Proceedings of the 23rd international conference, Venice, Italy; 1992. p. 512–25.
[44] Sunde A. Kjempebølger i Nordsjøen. Vær og klima 1995;18(1):17–23 [in Norwegian].
[45] Brodtkorb PA, Myrhaug D, Rue H. Joint distributions of wave height and wave steepness parameters, vol. 1. In: Proceedings of the 27th international conference on coastal engineering. Sydney, Australia; 2000. p. 545–58.
[46] Simons RR, Whitehouse RJ, MacIver RD, Pearson J, Sayers PB, Zhao Y, Channell AR. Evaluation of the UK Coastal Research Facility. In: Coastal dynamics'95: Proceedings of the international conference on coastal research in terms of large scale experiments, Gdansk, Poland; 1995. p. 161–72.
[47] Memos C. Stochastic description of sea waves. J Hydraulic Res 2002;40(3):256–74 [with contributions by Tzanis K, and Zographou K].
[48] Marthinsen T, Winterstein SR. On the skewness of random surface waves, vol. 3. In: Proceedings of the second international offshore and polar engineering conference, San Francisco, USA; 1992. p. 472–8.